Electrodeposition of Sn Rich, Au-Sn Solder Films

by

Charles Stuart Watt

A thesis submitted in partial fulfillment of the requirements for the degree of

Master of Science

in

Materials Engineering

Department of Chemical and Materials Engineering
University of Alberta

© Charles Stuart Watt, 2015

Abstract

Eutectic and near-eutectic tin (Sn) solder alloys have been indispensable when interconnecting and packaging electronic devices in the assembly of modern electronic circuits. Legislation has necessitated the implementation of lead (Pb)-free solder alternatives to replace near-eutectic Sn-Pb solders that were the most commonly used materials in the electronics industry. The Sn-rich eutectic alloy (90 wt% Sn) in the gold–tin (Au-Sn) system offers a potentially cheaper alternative to the Au-rich eutectic alloy (20 wt% Sn) for optoelectronic and microelectromechanical systems (MEMS) device packaging and may be applicable as a Pb-free solder for microelectronic packaging.

A simple electrodeposition method is utilized to fabricate Sn-rich, Au–Sn solder films, including the eutectic composition. The electrolyte is composed of a solution of Sn chloride and ammonium citrate. Gold is added to the electrolyte in the form of either a Au nanoparticle (<20 nm) suspension, prepared with Na citrate, or by directly adding Au powder (500–800 nm particles). The resultant electrolytes are used to electrodeposit eutectic and near-eutectic alloy films. Uniform thicknesses and compositions are obtained with the direct addition of Au powder. Gold content in the deposits increases with increasing Au particle loading in the electrolyte and increasing current density.

The intermetallic interactions and phase evolution in solder interconnections play an important role in the understanding the reliability and optimizing the solder process. The interactions between the Sn matrix and Au particles are examined. Room temperature aging leads to the formation of $AuSn_4$ at the Au particle-Sn matrix interface. Reflow of deposits with near-eutectic compositions results in the formation of Sn and $AuSn_4$.

Dedication

To my family,

thank you for both your love and support.

Charles

Acknowledgements

I would like to acknowledge the contributions of my supervisor Dr. Ivey for his time, support and guidance through the completion of my degree.

In addition, I acknowledge the help and guidance of Dr. Qi Liu, Dr. Anqiang He and Tina Baker for all of their assistance.

I would also like to acknowledge funding from Natural Sciences and Engineering Research Council (NSERC) of Canada and Micralyne, Inc.

Table of Contents

List of Tables

List of Figures

Chapter 1: Introduction

Gold-tin eutectic alloy solders are commonly used for optoelectronic device and microelectromechanical system (MEMS) packaging (Kim and Lee, 2005). The Au–Sn phase diagram has two eutectics, one which is Au-rich at 20 wt% Sn with a eutectic temperature of 280°C and another which is Sn-rich at 90 wt% Sn with a eutectic temperature of 217°C. The industry standard is the former eutectic, which is considered a hard solder, and has an excellent combination of mechanical and thermal properties (Kim and Lee, 2005). The Sn-rich eutectic composition is a potential lower cost alternative and may also be a candidate Pb-free solder for microelectronic applications, because of its relatively low melting temperature (217°C) (Kim and Lee, 2005 & Lee and Chuang, 2003). The Sn-rich eutectic does have some limitations, however. In particular, Sn-rich, Au–Sn alloys oxidize easily and the $AuSn_4$ intermetallic, which forms upon solidification after reflow, is brittle (Kim and Lee, 2005). However, according to Lee and Chuang (2003) the Sn-rich eutectic has suitable properties to be used for packaging applications, and its use would significantly reduce material costs. Several methods can be utilized to fabricate solder films.

Chapter 2 is the literature review presenting a life cycle analysis that outlines the legislations leading to Pb-free solder alternatives that will replace near-eutectic Sn-Pb solders most commonly used in the electronics industry. Of these methods, electrodeposition offers the best combination of cost effectiveness and process control particularly for solder deposited onto patterned wafers (Sun and Ivey, 1999). For the Sn-rich composition, a limited amount of work has been done, either through vacuum deposition or sequential electrodeposition of Au and Sn from two separate electrolytes (Jeong et al, 2006 & Kim et al, 2006 & Tang et al 2008 & He et al, 2012). The main concern with sequential electrodeposition is that deposits are exposed to air during transfer from one electrolyte to the other. This exposure is of particular concern for Sn, as it oxidizes readily in air. A recent publication has demonstrated that Sn-rich, Au–Sn alloys can be deposited from a single electrolyte consisting of Au and Sn chloride salts, as well as Na sulfite, ammonium citrate and other additives (He et al, 2012).

Chapter 3 outlines the experimental design used to create the electrolytes and the analytical techniques used to analyze the deposits. Small batches of the simple, “green”

electrolyte Sn electrolyte were prepared using Sn chloride and ammonium citrate (He and Ivey, 2008). Following the Sn electrolyte preparation, the electrolytes used in Chapters 4 and 5 are discussed. Lastly, each analytical technique used to complete the analysis of the deposits are described in detail.

Chapter 4 discusses the electrodeposition process using a simple, "green" electrolyte composed of a solution of Sn chloride and ammonium citrate developed previously (He and Ivey 2008). The addition of Au to the electrolyte occurs in the form of an Au nanoparticle (<20 nm) suspension prepared with sodium citrate.

In Chapter 5, a simpler approach is taken to electrodeposit Sn-rich, Au–Sn solders, including the Sn-rich eutectic. The same Sn electrolyte as that in Chapter 3 is used; however, Au is incorporated through the direct addition of Au powder (500–800 nm particles). Using Au particles keeps the solution simple, as there is only one species to be reduced.

Interactions between the Sn matrix and Au particles are examined in Chapter 6. Intermetallic interactions and phase evolution of the Sn-rich, Sn-Au solder films are discussed, specifically the as-deposited composition is compared with the composition after reflow. The importance of understanding the reliability and optimization of the solder process is discussed as well.

Chapter 7 summarizes the results for the work completed to develop a simple process for the electrodeposition of Sn-rich, Au-Sn solder films, highlighting the importance characteristics of the proposed Sn-rich Au-Sn solder composition while reinforcing the key results from the work. Lastly, potential future work is proposed.

Chapter 2: Literature

Life Cycle Analysis

Near-eutectic Sn-Pb solders were historically the most common soldering materials used in the electronics industry. Sn-Pb solders are desirable due to their low melting temperature, good workability, ductility, and excellent wetting (Evans, 2007). Eutectic and near eutectic tin lead alloys had become indispensable when interconnecting and packaging electronic devices in the assembly of modern electronic circuits. However, Pb processing and reclamation can have negative effects on the surrounding environment. Moreover, Pb is toxic if ingested into the human body. Major steps have been taken to reduce or eliminate Pb from specific fields in the industry. The European Union directives on Waste Electrical and Electronic Equipment (WEEE) state that components sold in the European Union must be Pb-free as of July 1, 2006 (Nimmo, 2002 & Gamalski, 2002). Major firms in Japan have been following the Japanese Ministry of Trade (MITI) legislation, which proposed take-back legislation in 1998 requiring manufactures to recover harmful materials in consumer grade production. Further reduction of harmful materials was mandated by MITI, which determined that the amount of lead used in commercial grade electronics must be reduced by half from 1996 to 2000 and to one-third by 2005 (Le Fevre, 2002). Korea has also started to develop products including handhelds and white goods with alternative alloy solders attempting to reduce Pb consumption (Evans, 2007). Within the United States, the Environmental Protection Agency has no official legislation on this matter but rather has strongly encouraged manufactures to reduce their hazardous wastes (Ku, 2003). To achieve these goals, potential replacements for Sn-Pb solder alloys include binary, ternary, and some quaternary alloys of Sn using Ag, Zn, In, Sb, and Cu (Evans, 2007). Legislation has led to Pb-free solder alternatives and further studies have been completed on these systems looking at the potential environmental and human impacts. These studies have involved a total Life Cycle Analysis (LCA) of Pb-free solders (Ku, 2003 & Turbini, 2001 & Zhou, 2008). This design approach uses the philosophy of industrial ecology by means of studying economics, green engineering, and sustainable development.

> The concept of industrial ecology is one in which economic systems are viewed not in isolation from their surrounding systems but in concert with them... As applied to industrial operations, it requires a systems view in which one seeks to optimize the total

> industrial materials cycle from virgin material, to finished material, to component, to product, to waste product, and to ultimate disposal. Factors to be optimized include resources, energy, and capital. (Wenzel, 1997)

A conventional LCA process can generate results subject to multiple interpretations. Despite this drawback, the advantages of this process enjoy wide recognition (Zhou, 2008). In practice, LCA analysis tends to stop at the level of inventory analysis or characterization (Zhou, 2008). Many other factors (economic, ideological, political, and social) are involved; the remaining steps of normalization, grouping, and weighting are not well defined in the global context (Zhou, 2008). Since conventional LCA processes are outside the scope of this thesis, only a brief description covering a LCA methodology for Pb-free solders is given as an introduction to the development of alternative solder materials. Ku (2003) used a qualitative, matrix based method developed by Allenby (1992) as the basis to compare information between Pb and six alternative metals (Ku, 2003). Designed and weighted metrics were created for toxicity and public health impact, availability and raw material supply, and environmental impact were compared to give supporting documentation to support decisions made in selecting alternative materials. However, depending on the required mechanic properties, each individual manufacturer can use other possible Pb-free solders as well.

Continuing with the LCA analysis, the next remaining stages can be investigated. A closer look at possible decision criteria such as processing methods, alloying systems, and current research in the field will be summarized.

Processing Methods

Processing methods used for mass manufacturing are important considerations when looking at possible new chemistries. Though there are a wide variety of application methods, the main processing method of focus is electrodeposition. Electrodeposition, or electroplating, is an economical and valid technology for producing solder deposits. Electrodeposition is the process of depositing a coating with specific characteristics by means of electrolysis (Lowenhein, 1974). The laws of electrolysis, formulated by Faraday, remain the foundation for this process. Simply

stated, electrodeposition is the reduction of a metal ion M^{z+} from an aqueous electrolyte represented by the following chemical reaction:

$$M^{z+} + ze^{-} \rightarrow M \quad (1)$$

Electrochemical cells are one of the basic tools that can be used to study processes and factors that affect the transport of charge across the interface between chemical phases (Bard and Faulkner, 2001). An electrochemical cell contains a reference electrode, a working electrode, and an ionic conductor (an electrolyte). The two electrodes are connected by a conducting wire through a power source. A potential difference is created by an external source, supplying additional electrons to the cathode or an electroless (autocatalytic) process in which the reducing agent in electrolyte acts as the electron source creating a reduction reaction (Paunovic and Schlesinger, 1998). Ions in the electrolyte are then attracted to the cathode where they are incorporated into the metal lattice (Lowenheim, 1974). Charge transport is achieved by the movement of electrons (or holes) and ions supplied by the electrolyte. The overall chemical reaction takes place in two independent half cell reactions at each electrode. However, the rate limiting step during practice is harder to determine since the electrolyte is being altered during deposition. The rates are driven by the potential differences existing at the metal-electrolyte interface (Lowenheim, 1974). For each system there is a specific potential and temperature for which the two competing rates are equal (Lowenheim, 1974). This equilibrium potential is dependent on temperature and concentration or activity of the ions in the electrolyte (Lowenheim, 1974). The equilibrium potential at the electrode where the reduction reaction from Equation 1 takes place is given by the Nernst Equation:

$$E = E^{0}_{M^{n+}} + \frac{RT}{nF} ln a_{M^{n+}} \quad (2)$$

in which E is the electrode potential, E^{o} is the standard potential of the reduction reaction, R is the gas constant, T is the absolute temperature, F is the Faraday's constant, η is the charge of the ion, and α is the activity of the metal ion in electrolyte. Variables, such as temperature (T), pressure (P), and ion concentration in the electrolyte are important for the consistent performance of any deposition bath. Small deviations can be sufficient to adversely affect plate quality, deposition rates, and other properties. In addition, the length of deposition time (t) controls the degree to which the reaction takes place.

Current efficiencies are important in practical applications, such as electrorefining and electroplating applications, where the mass of the metal deposited or dissolved is important (Paunovic and Schlesinger, 1998). In electroplating, current efficiency can depend on a number of parameters including: plating bath chemistry, pH, agitation, and current density (Paunovic and Schlesinger, 1998). Current efficiency (CE) mathematically, shown in Equation 3, is the ratio of the actual amount of metal deposited or dissolved, M_a, to the theoretically amount determined from Faraday's law, M_t.

$$CE = \frac{M_a}{M_t} \quad (3)$$

The applied potential (E) or current (i) are important considerations for electrodeposition methods and some of the main factors controlling the process. The amount of potential applied to the system can affect the quantity of electricity (Q), controlling which species in the electrolyte will react or be electrolyzed. Ideally the cathode and anode current efficiency should be equal leaving the electrolyte at a constant equilibrium. A deposit created in this ideal manner should have a specified brightness, hardness, ductility, and internal stress (Lowenheim, 1974).

The Metal-Electrolyte Interface

The metal-electrolyte interface involves two components: an electrode and an electrolyte in the case of an electrodeposition cell. Where the desired reduction reaction takes place is considered the "working electrode", while a "counter electrode" completes the circuit providing a standard reference that can be used to monitor potential changes in the system (Doesburg, 2000). At the "counter electrode", the following reactions can occur: metal dissolution, oxygen evolution, oxidation, or passivation (Doesburg, 2000). These interactions fall under two categories: Faradaic and non-Faradaic processes. Faradaic processes are governed by Faraday's law and involve reactions in which charges are transferred across a metal-electrolyte interface.

$$Q = nFN \ (4)$$

where Q is the quantity of electricity applied, n is the stoichiometric number of electrons involved in the chemical reaction occurring at the electrode, F is Faraday's constant (96485.3 coulombs/mole of electrons), and N is the number of moles electrolyzed.

Non-faradaic processes such as adsorption and desorption can occur at the electrolyte-electrode interface causing the electrode interface to change with changing potential or electrolyte composition (Bard and Faulkner, 2001). These processes occur when a charge does not cross the interface (Bard and Faulkner, 2001). However, external currents can flow when the potential, electrode area, or electrolyte composition changes (Bard and Faulkner, 2001). When no charge transfer occurs across the metal electrolyte interface, no matter the imposed potential caused by the external power source, the electrode is called an ideal polarized electrode (IPE) (Bard and Faulkner, 2001). The closest layer to the electrode contains solvent molecules and sometimes other species that are specifically adsorbed on the surface of the electrode (Figure 1). This "inner layer" is also known as the compact, Helmholtz, or Stern layer (Bard and Faulkner 2001). The electrical center of the specifically adsorbed ions is called the inner Helmholtz plane (IHP) at a distance x_1 (Bard and Faulkner, 2001). The solvate ions can approach only to a distance x_2, which in called the outer Helmholtz plane (OHP) (Bard and Faulkner, 2001). Nonspecifically adsorbed ions are distributed in the electrolyte extending from the OHP into the bulk of the electrolyte called the diffuse layer (Bard and Faulkner, 2001). Electrode processes will be affected by the structure of the double layer (Bard and Faulkner, 2001). Absorbed ions, solvated charges species, and oriented dipoles form at the interface of the electrode. This formation of charges species is referred to as the electrical double layer capacitance (Bard and Faulkner, 2001). An electrical double layer at the interface of the electrode and electrolyte can be approximated as a capacitor (Bard and Faulkner, 2001). In order for deposition to occur a charge must be applied to the electrical double layer to raise its potential to the required value for metal deposition (Bard and Faulkner, 2001).

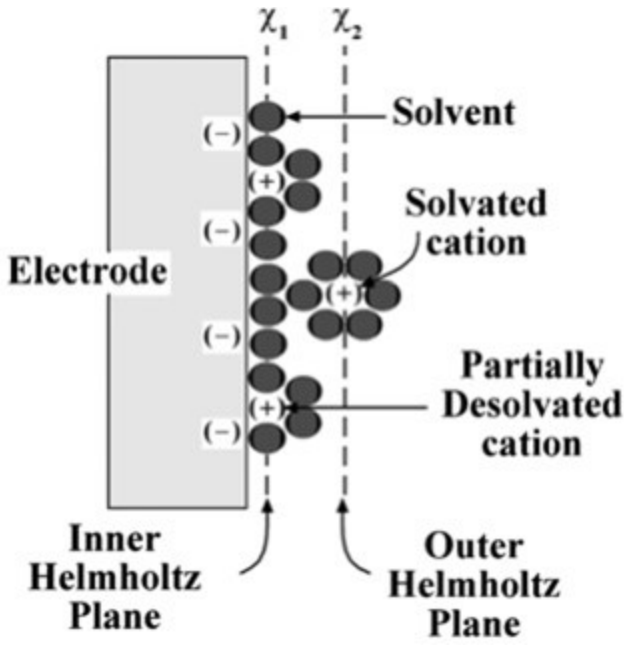

Figure 1: Schematic of the electrical double layer (Zoski, 2007).

Alloying Systems

Sn-Pb Systems

The majority of understanding with regard to electronic reliability comes from devices fabricated using Sn-Pb solders. Sn-Pb solders, specifically the 63 wt% Sn – 37 wt% Pb and 60 wt% Sn – 40 wt% Pb near eutectic solders (Figure 2), were the solder of choice at the beginning of electronics manufacturing. The metallurgy of the Sn-Pb alloy system is generally representative of all the soldering alloys in that it is a eutectic system. In a typical eutectic system, the solubility of one solid solution transitions to a much more limited solubility of the other alloying element. The highest temperature at which a metal or alloy is completely solid is called the solidus curve. While the lowest temperature at which the system is completely liquid is called the liquidus curve. At the extreme of the phase diagram are the pure metals. The temperature differential between the solidus and liquidus curves is called the melting or freezing range and within this range the alloy is partially melted or solidified. The two phases are usually distinguishable from one another and typically consist of layers or laminations to produce a "lamellar structure" consistent with a eutectic alloy.

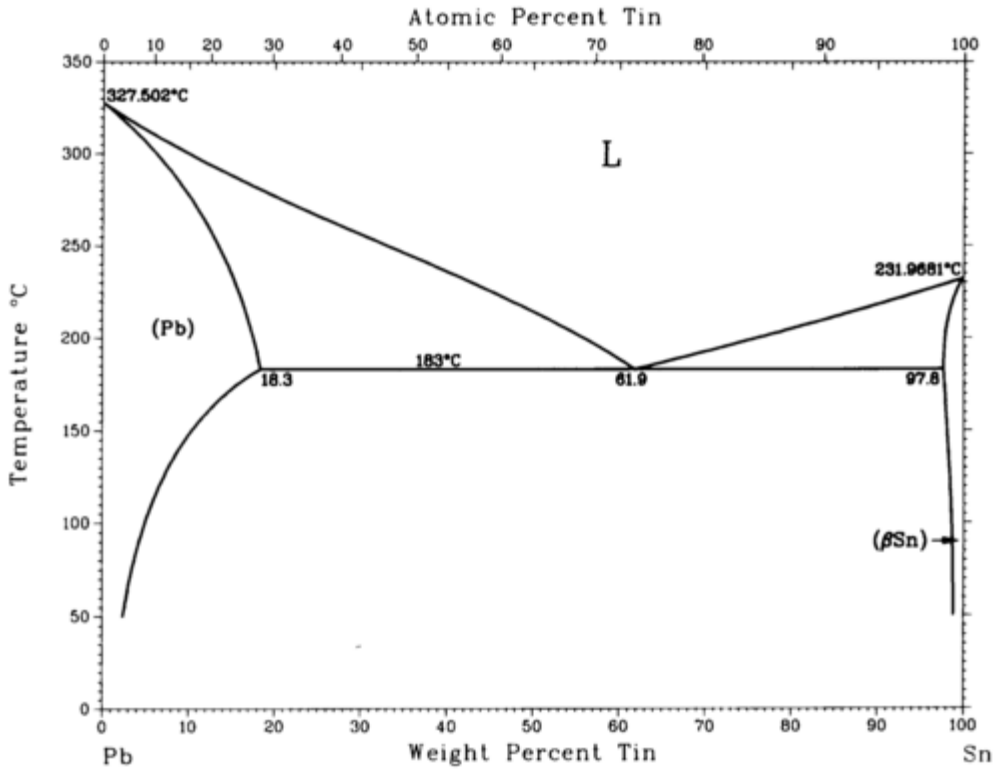

Figure 2: Pb-Sn binary phase diagram (American Society for Metals, 2012).

Sn-rich, Sn-Pb solder was chosen due to its superior properties among low melting point solders, superior manufacturing, and process compatibility (Evans, 2007). Near eutectic alloys of the Sn-Pb system are well suited for machine-soldering and mass-soldering methods and are still considered the best alternative for certain applications (Evans, 2007). There are many other important solder compositions in the Sn-Pb systems that should be highlighted:

- 5 wt% Sn – 95 wt % Pb solder composition has a relatively high melting temperature, has a narrow melting and freezing range, and is poor in terms of wetting and flow compared with higher Sn alloys. However, the mechanical properties of this high-Pb alloy are better at 149°C (300°F) than most other alloys with more Sn.
- The 10 wt% Sn – 90 wt% Pb, 15 wt% Sn – 85 wt% Pb, and 20 wt% Sn -80 wt% Pb solders have progressively lower liquidus and solidus temperatures, a wider melting range, and better flow than 5 Sn – 95 Pb. All are prone to solidification cracking or "hot tearing".

- The 25 wt% Sn – 75 wt% Pb and 30 wt% Sn -70 wt% Pb solders have lower liquidus temperatures than all previous, more Pb-rich solders. The melting range is thus narrower, so there is a lesser tendency toward hot tearing.
- The 35 wt% Sn – 65 wt% Pb, 40 wt% Sn – 60 wt% Pb, and 50 wt% Sn – 50 wt% Pb solders have low liquidus temperatures and, as a group, have the best combination of wetting, strength, and economy.
- The 60 wt% Sn – 40 wt% Pb solder is used whenever exposure temperature restrictions are critical for the assembly or some of its components, since the composition is close to the eutectic. It is cheaper because it contains slightly less expensive Sn than the true eutectic at 63 wt% Sn – 37 wt% Pb.
- The 70 wt% Sn – 30 wt% Pb alloy is a special-purpose solder used where a high Sn content is required for wetting or other compatibility.

Therefore, Pb-Sn solders are an excellent basis of comparison for alternative Pb-free solders.

Pb-free Systems

As previously mentioned, substitutes for Pb are being investigated for Sn-Pn solder alloys. Primarily, candidates tend to be composed of near-eutectic or eutectic alloys which provide the best manufacturable capability (Evans, 2007). Although, no direct substitute has been found, candidate systems have been considered for alloys Sn-Ag, Sn-Cu, Sn-Sb, Sn-Zn, Sn-In, and Sn-Bi. In and Bi alloys lower the melting point considerably and produce inferior mechanical properties in comparison with the Sn-Pb system. Zn may be used in speciality processes where Zn drossing rates or corrosion resistance are not high priority issues. Cu has been used as a low cost replacement by Nortel (Trumble, 1998) and demonstrated successful manufacturing capability. Ag has improved mechanical properties and wettability when compared to Cu, but has limited applications due to cost and availability. Ternary and quaternary alloys have shown superior performance in comparison with Sn-Pb systems. However, highly alloyed systems may demonstrate segregation or reproducibility of composition issues and may require specialized processing methods. A summary of possible replacement alloys and industrial applications is shown in Table 1.

Table 1 Composition and Application Data for Selected Solders (Evans, 2007)

Alloy System	Nominal Composition of Selected Alloys (wt%)	Melting Range (°C)		Application Remarks
		Solidus	Liquidus	
Sn-Pb	63wt%Sn37 wt%Pb (e)	183	183	Primary joining alloy for electronic assembly.
	60 wt%Sn40 wt%Pb	183	191	
	62 wt%Sn36 wt%Pb2 wt%Ag (e)	179	179	
Pb-Sn	95 wt%Pb5 wt%Sn	308	312	High-temperature solders for die attachment.
	90 wt%Pb10 wt%Sn	268	301	
Pb-Sn-Ag	97.5 wt%Pb1 wt%Sn1.5 wt%Ag (e)	305	305	
	82.5 wt%Pb15 wt%Sn2.5 wt%Ag	275	280	
Pb-In	75 wt%Pb25 wt%In	226	264	High-temperature solders.
	50 wt%Pb50 wt%In	180	210	
Sn-Ag	96.5 wt%Sn3.5 wt%Ag (e)	221	221	Primary replacement candidates for near-eutectic SnPb alloys; high melting point.
Sn-Ag-Cu	95.5 wt%Sn3.8 wt%Ag0.7 wt%Cu (e)	217	217	
	95.5 wt%Sn3.9 wt%Ag0.6 wt%Cu	~217	~217	
Sn-Bi	42 wt%Sn58 wt%Bi (e)	138	138	Low melting point eutectic; potential segregation problems; low melting temperature phase with trace of Pb.
Sn-Bi-Ag	93.5 wt%Sn3 wt%Bi3.5 wt%Ag	206	213	Replacement candidates for near-eutectic SnPb alloys; potential segregation and cracking problems with increasing Bi content; low melting point phase with trace Pb.
	91.5 wt%Sn5 wt%Bi3.5 wt%Ag	-	-	
	90.5 wt%Sn7.5 wt%Bi2 wt%Ag	207	212	
	76 wt%Sn22 wt%Bi2 wt%Ag	-	-	
Sn-Bi-In	70 wt%Sn20 wt%Bi10 wt%In	189	199	

Sn-Cu	99.3S wt%n0.7 wt%Cu (e)	227	227	Low cost; plumbing alloy; poor mechanical properties.
Sn-Zn	91 wt%Sn9 wt%Zn (e)	198.5	198.5	Zn imparts poor corrosion resistance and reduced wettability; Zn has low vapor pressure leading to segregation in wave pots; Ag alloying may improve SnZnIn ternary properties; Cu alloying may improve SnAgZn.
Sn-Zn-Bi	89 wt%Sn8 wt%Zn3 wt%Bi	189	199	
Sn-Zn-In	87 wt%Sn8 wt%Zn5 wt%In	~188	~188	
Sn-Zn-Ag	95.5 wt%Sn1 wt%Zn3.5 wt%Ag (e)	217	217	
Sn-In	48 wt%Sn52 wt%In	117	117	In adds cost; specialized applications for wetting ceramics and glasses.
	50 wt%Sn5 wt%0In	117	125	
Sn-In-Ag	77.2 wt%Sn20 wt%In2.8 wt%Ag			
In-Ag	90wt%In10 wt%Ag	141	237	High cost
Sn-Sb	95 wt%Sn5 wt%Sb	235	240	

Au-Sn System

Gold's high electronic conductivity, low contact resistance, and good solderability make it an ideal choice for electrical and electronic hardware (Reid, 1974). An Au-rich, Au-Sn eutectic solder is often used for specialty applications. The 80 wt% Au 20 wt% Sn eutectic solder is composed of ζ (Au_5Sn) and δ (AuSn) with a eutectic temperature of 278°C (Figure 3) (American Society of Metals, 2012). This Au-rich eutectic composition is classified as a hard solder due to the high melting temperature of Au. Analysis has shown that the Au-rich eutectic composition has good creep behaviour and creep resistance (Reid, 1974 & Sun and Ivey, 2001). Furthermore, due to its high electrical conductivity, low contact resistance, and good solderability, 80Au20Sn has been used for specific applications in electronics (Reid and Goldie, 1974).

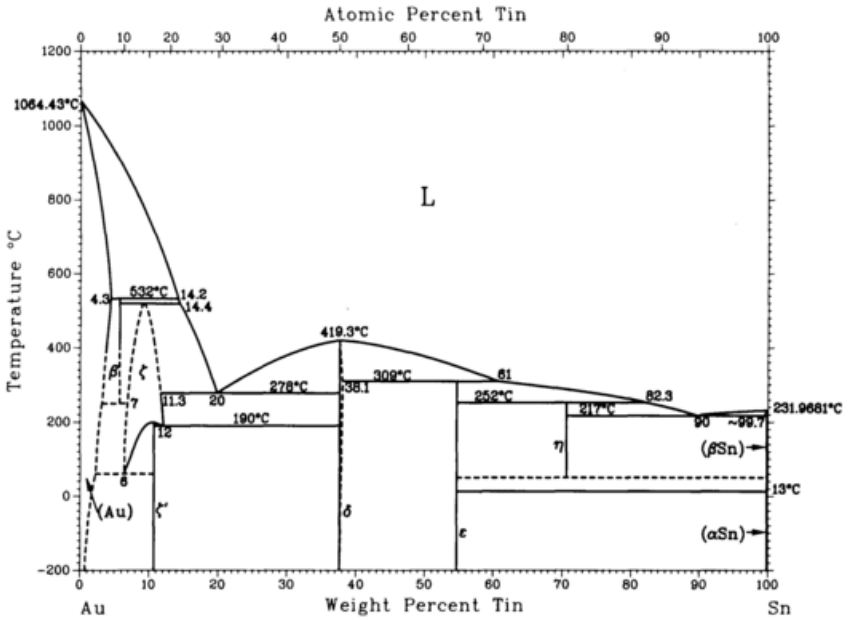

Figure 3: Au-Sn binary phase diagram (American Society for Metals, 2012).

An-Sn Solders

Au – Sn eutectic solders have been produced in sequential layers by depositing an Au seed layer followed by a Sn layer (Kallmayer et al, 1995 & Zakel et al, 1995). Au and Sn electrolytes are readily available commercially and are utilized to deposit these layers. Au and Sn co-deposition from a single electrolyte offers an economical advantage over sequential plating. Electroplating electrolyte chemistries can be altered to stabilize the co-deposition bath. Both acidic and alkaline electrolytes have been developed, with the primary focus towards acidic electrolytes for co-deposition of the Au-Sn system.

Co-deposition from a cyanide system using pyrophosphate as a buffering agent has been studied with a basic formula consisting of $K_4P_2O_7$, $KAu(CN)_2$, and $SnCl_22H_2O$ (Kubota, 1983). The investigation was focused on the mass transfer reaction mechanisms between monovalent Au or bivalent Sn and pyrophosphate ions by measuring conductivity, kinematic viscosity and limiting current density of eletrodeposition (Sun & Ivey, 1999).

Various Au-Sn compositions have been electrodeposited from cyanide electrolytes containing $HAuCl_4H_20$, $K_2SnO_33H_2O$, KCN, and KOH. Investigation did not yield a linear

relationship between the Sn content in the electrolyte and the Sn content formed in the deposit. Instead a relationship was found between the two alloys, which permitted formation of the desired compositions (Tanabe et al, 1983). Development of non-cyanide based electrolytes has been challenging, yet has yielded some success. A major challenge with the development of non-cyanide electrolytes is the lack of a strong Au complexing agent. Other challenges in co-deposition of the Au-Sn system can arise due to the oxidation of stannous ions to stannic ions in the electroplating bath - such oxidation can be caused by either atmospheric oxygen or anode oxidation (Schlesinger and Paunovic, 2000).

Sn-Rich, Sn-Au Solders

The Au-Sn system has a second eutectic composition, which is Sn-rich and shown in Figure 3, that may be a candidate Pb-free solder to be used in microelectronic applications. The Sn-rich, Sn-Au solder composition is not currently used in the industry. This allows for the opportunity to explore an alternative composition for solder joints in optoelectronic and MEMS applications and to develop cheaper alternatives to the Au-rich solder (Lee, 2003 & Lee, 2005). According to Lee, 2003 the Sn-rich eutectic composition has suitable properties to be used for packaging applications, and its use would significantly reduce material costs. Its most interesting property is its ability to plastically deform under stress without failing under normal usage. Tang, 2008 explored solidification and intermetallic formation of Sn-Au couples. This particular composition range does have some drawbacks, however, as Sn-rich, Sn-Au alloys oxidize easily and the $AuSn_4$ intermetallic that forms upon solidification after reflow is often brittle (Lee, 2005).

Gold Electrodeposition

The type of electrolyte can be further classified depending on the basis of application. Whether Au is being deposited for its color or industrial use will affect the technological requirements (Reid,1974). “Color golds” have a limited interest in the field and are typically used in thin “flash like” deposits. “Industrial golds” are used for functional purposes where processes are described as pure Au or bright alloy Au (Reid, 1974). Initially, industrial baths containing 22.5 - 26 g/L of Au were recommended (Volk, 1957 & Raub, 1967). Pure Au electrolytes have not changed much since the 1960s; additions of potassium hydroxide and the

use of ammonium gold cyanide with the application of ultrasonics have made improvements (Reid, 1974). Bright alloy Au deposits involve the codeposition of Ag, Sn, and Sb (Reid, 1974).

Alkaline Cyanide Baths

Originally alkaline baths were used for commercial Au plating, i.e., since the 1840's (Foulke, 1969). Alkaline cyanide baths operate at a high pH with an excess of free cyanide. Typically, potassium gold cyanide is used as a source of free cyanide in these baths. The cyanide released during the deposition does not significantly alter the cyanide concentration in the bath. Shifting the potential of Au (I) cyanide due to accumulation of free cyanide does not occur. The excess cyanide permits the use of gold anodes for the replenishment of the metal plated from the bath:

$$\text{Cathode: } [Au(CN)_2]^- + e^- \rightarrow Au + 2CN^-$$

$$\text{Anode: } Au + 2CN^- \rightarrow [Au(CN)_2]^- + e^-$$

$$\text{Full cell: No change to plating electrolyte}$$

The main changes that occur in the bath are due to oxidation or reduction side reactions, drag-out of plating salts, and drag-in of water or impurities. The free cyanide promotes the corrosion of the gold anode forming $[Au(CN)_2]^-$, increases the throwing power, and improves the conductivity.

Neutral Cyanide Electrolytes

Non-alkaline baths exhibit a wider range of physical and chemical properties than possible at higher pH levels. Although the metals used to harden Au are not readily codeposited from neutral pH baths, they can be formed using a careful selection of plating parameters without the use of additives. In neutral baths the gold salt used is the same as for alkaline and acid baths, $KAu(CN)_2$. Neutral pH and the absence of free cyanide create favorable formulations for the use of photoresist and other polymeric materials. Typically, a pure soft gold can be produced using neutral baths at relatively low current densities. The phosphate salts serve as a supporting electrolyte and pH control causing less concern regarding concentration control.

Additive free hard gold (AFHG) can be produced from neutral baths using phosphate as the buffer. The advantages of AFHG baths over metal hardened baths are:

- No need to control additive concentration;
- High current efficiency;
- Greater tolerance for heavy metal impurities due to the insolubility of many metal phosphates;
- High ductility and thermally stable contact resistance for electronic components.

Although there are advantages to AFHG baths, there are some susceptibilities to contamination, mainly to small impurities such as Ni, Co, and Fe ions that can cause large changes to the physical properties of the deposits.

Acid Cyanide Electrolytes

These electrolytes were originally developed for the jewelry trade but are now being used throughout the electronics industry. An advantage of using acidic electrolytes is that photoresist and other polymers can be used as templates (Foulke, 1969). Typically, platinized Ti, Au, or Au-plated platinized Ti are used for the anodes in these baths. The use of gold plated electrodes is found to not readily dissolve at low current densities due to a low free cyanide concentration created at low current densities. If high current densities and a low electrolyte volume are present, concentrations of free cyanide can build in the electrolyte and lead to oxidation and dissolution of a pure gold or gold plated anode. In these situations insoluble anodes can be used with additions of plating salts to replenish the gold content and maintain pH control. It is recommended to avoid stainless steel and carbon anodes because they can introduce contamination into the system.

Acid cyanide baths allow for the codeposition of other metals easily with gold, resulting in physical property changes especially hardness of the deposits. Hard gold is highly important to electronic components where low contact resistance, pore-free deposits, wear resistance, and chemical inertness are functional requirements. Hard deposits can be produced containing cobalt, nickel, indium, silver, arsenic, or cadmium. When using acid cyanide baths, the most reliable finish can be achieved with either nickel or cobalt salts.

Non-Cyanide Electrolytes

Commercial gold sulfite baths have been given special attention do to the effect of the plating temperature and current density on residual stress in the deposit. Although Au sulfite has

been used in commercial baths, the complex is susceptible to disproportionation, forming Au (III) and metallic gold. Since, spontaneous decomposition of the bath may occur this has led to the development of proprietary stabilizing additives.

Tin Electrodeposition

The most common complexing agents in pure Sn electroplating electrolytes are fluoboric acid, sulfuric acid, phenolsulfonic acid, hydrochloric acid, hydrofluoric acid, and methane sulfonic acid (Schlessinger and Paunovic, 2000). The type of complexing agent used will affect the performance and application of the Sn electrolyte. Tin electrolytes can either be acidic or alkaline in nature. Whether acidic or alkaline electrolytes are used depends on the specific requirements of the application. Acid baths use stannous sulfate or stannous fluoborate. Allowing the process to occur at room temperature, use relatively low current densities, and deposition occurs in the bivalent state (Zhang, 2010). Acid baths do have disadvantages of requiring addition additives and a lower throwing power. Alkaline baths use sodium or potassium stannate as the source of Sn. Wide ranges of concentrations have been used to regulate the rate of plating making the composition formulation relatively simple. Alkaline baths are known to have excellent throwing power and insoluble anodes can be used (Zhang, 2010). However, higher current densities must be used since Sn is plated from the trivalent state as well as the baths must be heated.

Fluoborate Chemistry

Fluoborate chemistry is one of the oldest electroplating acid tin chemistries and is typically used in high-speed plating (Zhang, 2010). Organic additives most commonly used in fluoborate chemistry are peptone, gelatin, β-naphthol, catechol, and hydroquinone. Typical bath compositions are listed below, and when these compounds are added the result is a fine, smooth deposit. The advantages of fluoborate chemistry are its ability to operate at high current densities and its high throwing power and high current efficiency at both the anode and cathode. The major disadvantage of fluoborate chemistry is the environmental concerns associated with the fluoride and boric ions.

Table 2 Typical Fluoborate Electrolyte Chemistries (Zhang, 2010)

Parameters	Rack and Barrel	Reel to Reel
$Sn(BF_4)_2$, g/L	75-113	225-300
Sn, g/L	30-45	45-60
HBF_4, g/L	188-263	225-300
H_3BO_3, g/L	22.5-37.5	22.5-37.5
Anode current density, ASF	20-25	Do not exceed 25
Cathode current density, ASF	1-80	Up to 300
Temperature, °C	30-55	30-55

Sulfate/Sulfuric Acid Chemistry

One of the characteristics of sulfate/sulfuric acid electrolyte chemistry is its current efficiency at both the cathode and the anode under normal operating conditions (Zhang, 2010). This chemistry is cost-effective and is relatively easy to maintain and control because of the following reaction:

$$SnS0_4 + H_2O \rightarrow [Sn(OH)]^+ + HSO_4^-$$

Deposits may range from matte to semi-bright to bright by using a variety of additives. The disadvantages of sulfate chemistries are passivation at high current density and the tendency to corrode the plating equipment.

Table 3 Typical Sulfate/Sulfuric Acid Electrolyte Chemistries (Zhang, 2010)

Parameters	Range
$SnSO_4$, g/L	15-45
Sn, g/L	7.5-22.5
Sulfuric acid, g/L	135-210
Additives	Alkylphenol, imidazonline, heterocyclic aldehydes
Anodes	Pure Sn
Anode current density, ASF	25 max
Cathode current density, ASF	1-25
Temperature	Room Temperature
Agitation	Mechanical, cathode rod

Phenolsulfonic Acid and Halogen Electrolytes

Phenolsulfonic acid and halogen electrolytes are the two most commonly used chemistries to plate pure tin in the continuous steel strip plating industry (Zhang, 2010). Typical formulations and operating conditions are shown below.

Table **4** Typical Phenolsulfonic Acid Electrokyte Chemistries (Zhang, 2010)

Parameters	Range
Sn, g/L	20-35
Phenolsulfonic acid, g/L	40-80
Additives	Ethoylated β-naphtholsulfonic acid
Antioxidant	-
Current Density, ASF	200-500
Temperature, °C	30-40

Table 5 Typical Halogen Electrolyte Chemistry (Zhang, 2010)

Parameters	Range
NaF, g/L	30
$NaHF_2$, g/L	31
SnF_2, g/L	19
$SnCl_2 \cdot 5H_2O$, g/L	22
$Na_2Fe(CN)_6 \cdot 10H_2O$, g/L	2-4
Additives	Naphtholsulfonic acid and polyalkyelen oxides
Antioxidant	$_p$-$NH_2C_6H_4NHCOMe$
pH	3-4
Current density, ASF	200-500
Temperature, °C	55-65

The benefit of either of these processes is their ability to operate at very high current densities, which is an advantage in the steel industry. Phenolsulfonic acid processes use a vertical cell design with either a soluble or insoluble anode, whereas the halogen process uses a horizontal cell design with a soluble anode. Both processes, however, cause sludge formation and environmental issues have brought about the development of an alternative methanesulfonic acid-based process that is more environmentally benign.

Methanesulfonic Acid Electrolyte

Proell recognized the electroplating applications of methanesulfonic acid as an electrolyte in the 1940s, although it was not readily accepted until the early 1980s. Methanesulfonic chemistry has shown clear advantages over the previously described electrolytes using fluoborate, sulfate, halogen, and phenolsulfonic acids. The conversion from Sn (II) to Sn (IV) is less of a problem than for fluoborate/sulfate chemistries and is less costly than the previously described fluoborate, PSA, and halogen chemistries.

Research by Ivey et al

Ivey et al. have been working on electrodeposition of the Au-Sn system for packaging microelectronics and optoelectronic devices. Currently, Ivey et al. has developed methods for co-deposition and sequential deposition of Au-rich, Au-Sn solders on both patterned and un-patterned substrates. Co-deposition studies were completed using a non-cyanide based electrolyte containing five major components: $KAuCl_4$, $SnCl_2{\cdot}2H_20$, tribasic ammonium citrate $(NH_4)_3HC_6H_5O_7$, sodium sulfite (Na_2SO_3), and ascorbic acid ($C_6H_8O_6$). Sequential deposition studies were completed using separate and simple Au and Sn electrolytes. The Au electrolyte contained $(NH_4)_3HC_6H_5O_7$, $KAuCl_4$, and Na_2SO_3, whereas the Sn electrolyte contained $(NH_4)_3HC_6H_5O_7$and $SnCl_2{\cdot}2H_2O$.

Sun and Ivey (1999) initially investigated the electrolyte chemistry used for co-deposition of Au-Sn solders and their investigation led to the development of the co-deposition electrolyte mentioned above. They determined that the Au-Sn plating bath stability depended on the total Au and Sn content, additive content, and how the electrolyte was prepared and stored. The resulting deposits were compared using pulse current and direct current plating techniques, demonstrating that a pulse current using a duty cycle of 20% produced finer and smoother microstructures (Sun and Ivey, 2001).

Doesburg and Ivey (2000) continued to study the co-deposition of the Au-Sn system using the electrolyte developed by Sun and Ivey. They studied the effects of average current density on the microstructure and preferred orientation of the deposit. The preferred orientation was related not only to the microstructure produced but also to the phase or phases that were present in the deposit. The average current density used controlled the phases formed during electrodeposition. Djurfors and Ivey (2002) showed that changes in average current density could produce multilayered deposits with multiple phases present in the solder structure. This multilayer structure created was composed of two stoichiometric phases: AuSn and Au_5Sn (Figure 4).

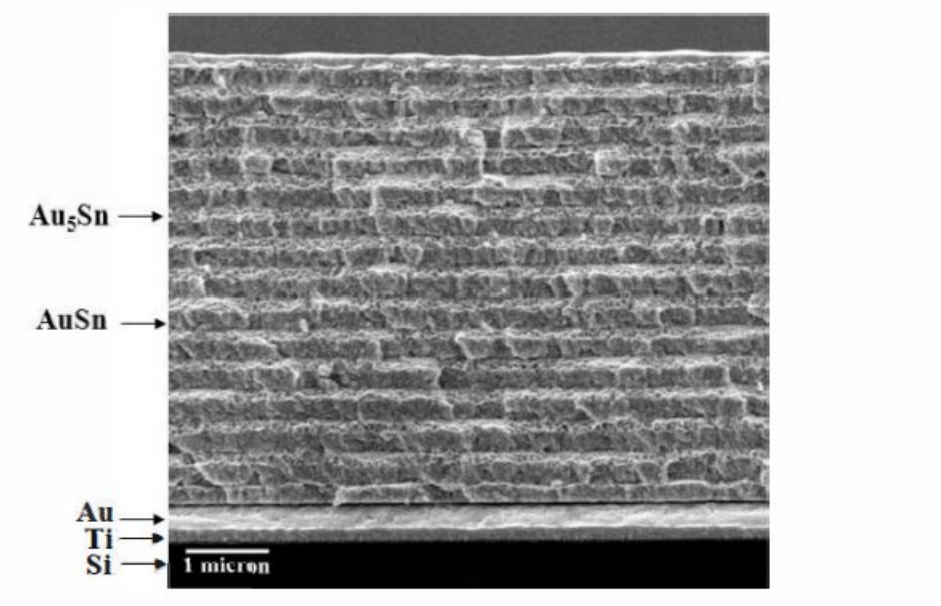

Figure 4: SEM SE image showing the multi-layered deposit produced by Djufors and Ivey. Each layer was deposited in sequence at 2.4 mA/cm^2 for 5 min and 0.8 mA/cm^2 for 21 min (Djurfors & Ivey, 2002).

Zhang and Ivey (2004) investigated the effect of additives to the plating bath, specifically the effect of ammonium citrate on plating rate, deposit composition, and morphology. They determined that lowering the ammonium citrate concentration produced smoother and denser deposits. Morawej and Ivey (2007) further optimized the plating bath, as they studied the long-term stability of the standard electroplating bath developed by Ivey's group. Together they determined that electrolyte depletion affects the amount of compositional change in the deposits over time; the morphology becomes rougher and less dense as the electroplating electrolyte ages, and the storage methods of the electroplating electrolyte affect the composition and morphology of the deposit. The major constituent that affected the stability of the Au-Sn system was the amount of ammonium citrate added to the electrolyte, while the Au and Sn concentrations in the electrolyte did not affect the stability but rather the deposition rates. Simulations were done using a Box-Behnken design type to obtain an optimal electrolyte chemistry. This resulted in an electroplating electrolyte with an improved plating rate (by four times) at the eutectic composition and the electrolyte had a shelf life of two days.

Tang and Ivey (2008) investigated the effects of sequential electrodeposition on the Au-Sn system using the standard electroplating bath electrolyte described earlier. Sequential deposition in comparison with co-deposition can be an advantageous process method. A key difference between the two methods is the difference in the stability of the electroplating electrolyte. The co-deposition electrolyte has a shelf life of three days, while the separate Au and Sn electrolytes have shelf lives of at least three months. As such, sequential electrodeposition of the Au-Sn system maybe a more cost-effective method and may be easier to implement and control for commercial processes. Tang and Ivey (2008) also investigated the effects of deposition order and the resulting microstructures of Au-rich and Sn-rich, Au-Sn solders alloys. Tang et al. (2008) studied the room temperature interface reactions of sequentially electrodeposited Au/Sn couples shown in Figure 5 and Figure 6. They determined that the order in which the Sn and Au layers were sequentially deposited affected intermetallic formation. Intermetallics $AuSn_4$ and AuSn were formed in Au/Sn couples when Au was the first layer to be deposited. Au_5Sn and AuSn were the intermetallics formed in Au/Sn couples when Sn was the first layer deposited.

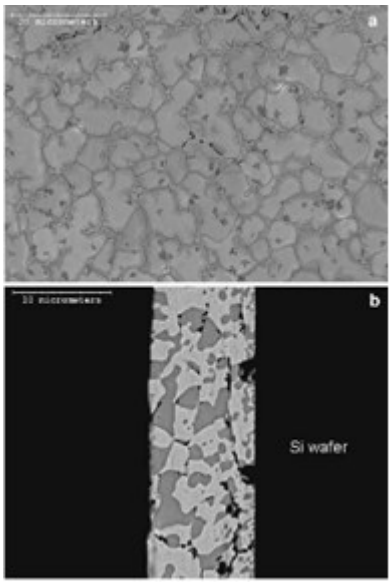

Figure 5: SEM backscattered electron (BSE) plan view image (a) and cross sectional image (b) of the Au-rich, eutectic Au-Sn alloy after reflow at 320°C for 5 min (Tang, 2008).

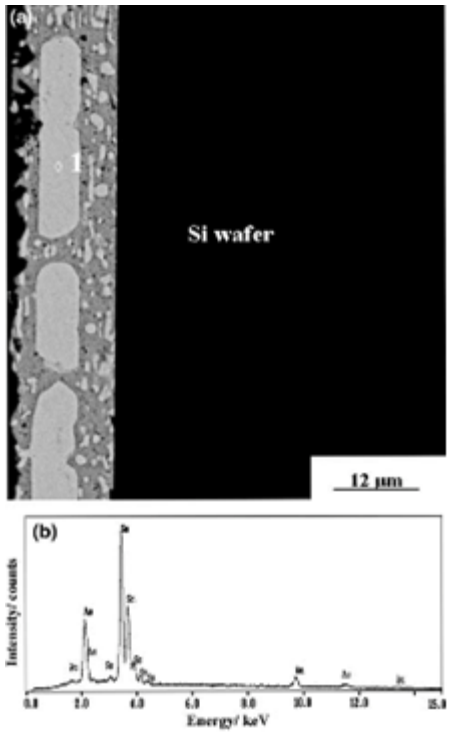

Figure 6: SEM BSE cross-sectional image (a) and EDX spectrum (b) from the proeutectic phase of a Sn-rich, hypoeutectic Au-Sn alloy (point 1) after reflowing at 250°C (Tang et al., 2008).

Research by Lee et al

Lee et al. (2002) have investigated the possibility of using Sn-rich, Au-Sn solders in electronic and photonic packaging applications. They have studied Sn-rich, Au-Sn bonding processes in reducing atmospheres and ambient air. The Sn-rich, Au-Sn solder composition can be advantageous relative to hard solders typically used in these applications. Hard solders such as the Au-rich, Au-Sn solder have very high yield strengths, which would incur only elastic deformation rather than plastic deformation under stresses in normal usage. A lack of plastic deformation could result in the inability to release stresses developed in the structure causing a catastrophic failure. Soft solders, on the other hand, such as Sn-rich, Au Sn solders are susceptible to thermal fatigue and creep movement, something that hard solders do not experience.

Lee et al. 2006 have looked at a fluxless flip-chip bonding process using a hydrogen environment to produce Sn-rich, Sn-Au solder bumps. Sn-Au multilayered structures were deposited using sequential deposition techniques on metallized wafers containing a Cr/Au seed

layer. A Sn layer was deposited first followed by an Au layer to prevent Sn oxidation. The Sn layer was deposited using a stannous Sn-based electrolyte with a bath temperature of 46°C and a pH of 1. A current density of 21.5 mA/cm^2 was used for 85 min to produce a 40 μm layer of Sn. The gold was deposited directly after tin deposition. The Au electrolyte was a neutral non-cyanide electrolyte and Au was deposited at 60°C with a current density of 4.6 mA/cm^2.

The resulting morphology after sequential deposition is shown in Figure 2.13. Figures 7a and 7b show the initially deposited Sn layer on the Cr/Au metallized wafers. Figures 7c and 7d show the morphology after the Au was deposited on the initial Sn layer. The deposited Au should have a 0.2 μm thickness assuming a smooth Sn deposit. However the Au was deposited preferentially along the Sn grain boundaries (Lee and Kim, 2005). Cross-sectional images (Figure 8) were taken to show that the Au clusters preferentially deposited along the ridges of the deposited Sn grains.

Kim and Lee (2008) created a Sn-Au sequentially plated solder joint, as shown in Figure 9. The Sn-rich, Sn-Au solder film was reflowed using a bonding temperature of 250°C. Analysis after solidification showed that the eutectic phases, Sn and $AuSn_4$, had formed.

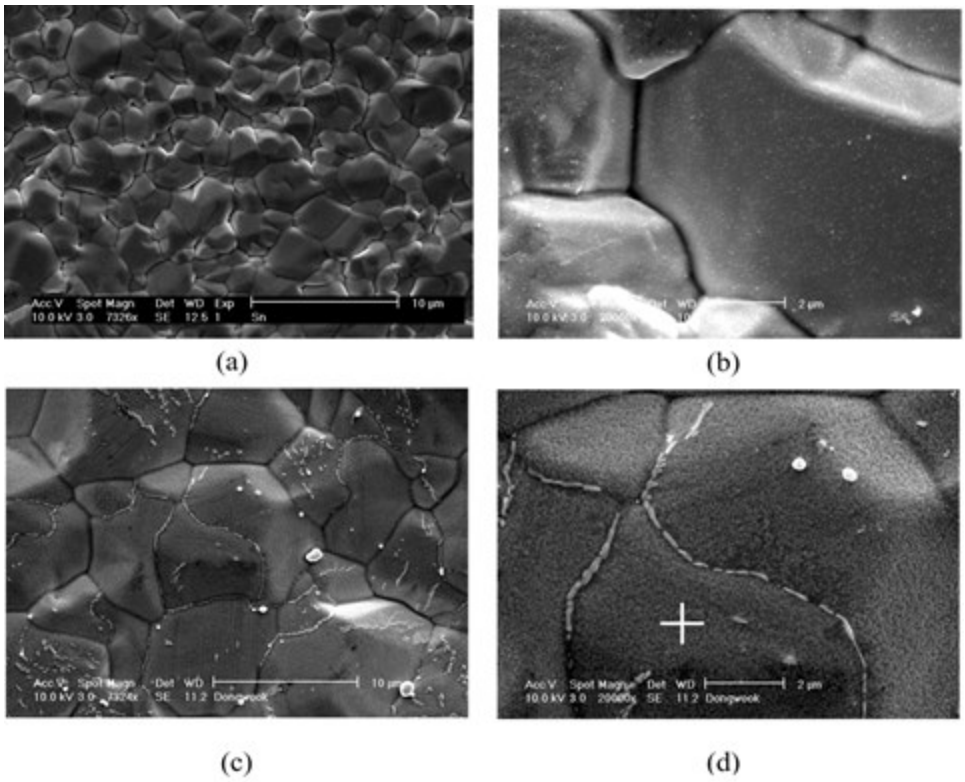

Figure 7: Plan view SE images of the sequentially deposited layers. a) Low magnification image of the as-deposited Sn layer; b) high magnification image of the as-deposited Sn layer; c) low magnification image of the deposit after Au deposition; d) high magnification image of the deposit after Au deposition (Kim and Lee 2006).

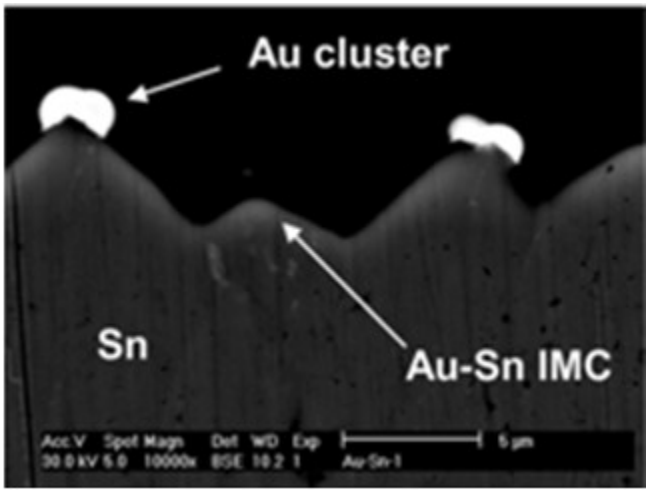

Figure 8: Cross-sectional BSE image of a sequentially deposited Sn-Au solder film (Kim and Lee, 2006).

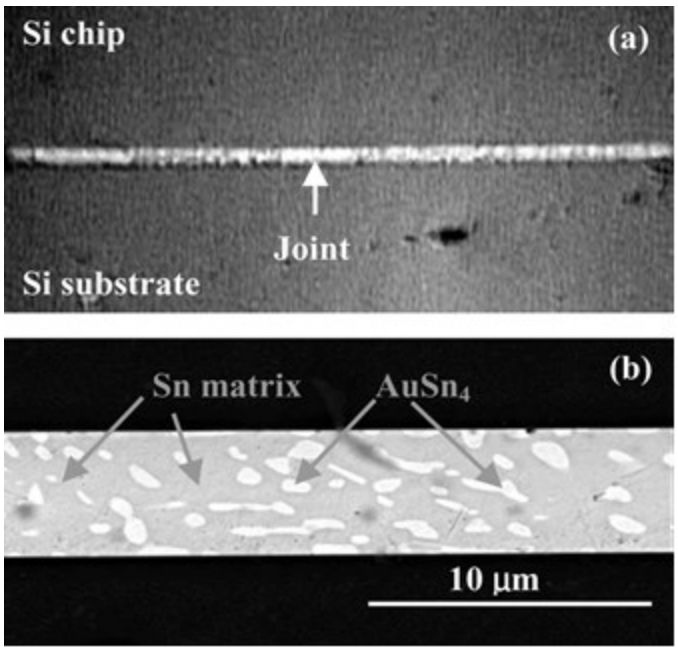

Figure 9: Sn-rich, Sn-Au reflowed soldered joint. a) Optical microscope image and b) SEM BSE image (Kim and Lee 2006).

Research by Barkey

Barkey and his group have been developing Sn-based solders for semiconductor packaging. They have used elecrodeposition techniques in order to deposit the solder alloys. Electrodeposition is used because it provides thickness control and can be easily scaled down for small batch testing. In order to better understand the electrodeposition of Sn-rich, Ag-Sn alloys, his group has investigated the possibility of co-deposition of a Sn-Ag alloy with a Ag electrolyte and Ag particles (Barkey, 2006).

Barkey used a planar stainless steel rotating disk electrode (RDE) to deposit Sn-Ag solder alloys from a commercial pure tin bath (Rohm and Haas Solderon BP Acid) with additions of silver particles (0.5 – 1 μm in size). The additions of silver particles in the Sn electrolyte ranged from 1 to 8 g/L. Barkey proposed that the silver particles were deposited onto the surface and then incorporated into the solder film by Sn depositing over the Ag, as shown in Figure 10. Two different morphologies were obtained. The first morphology resulted from an Ag particle loading between 1 and 4 g/L. These deposits, shown in Figure 11a, appeared to produce solder

bump with the amount of Ag particles incorporated being negligible. The second morphology was due to Ag particle loading between 4 and 8 g/L. The deposits, shown in Figure 11b, had a "mossy" like structure composed of 25 to 75 wt% Ag on top of the solder bump.

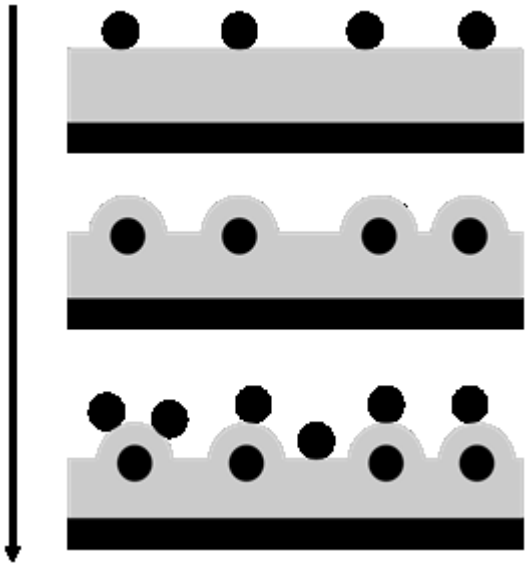

Figure 10: Proposed deposition sequence (Barkey, 2006).

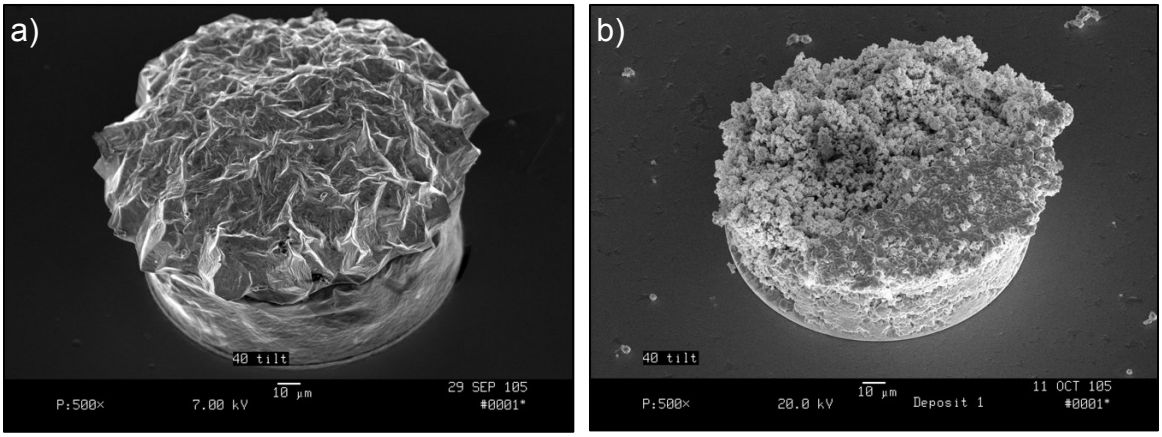

Figure 11: Sn-Ag deposited solder bumps. a) Particle additions less than 4g/L and b) particle additions greater than 4 g/L (Barkey, 2006).

Applications

With the directive of reducing and eliminating Pb-based solders, Pb-free solders have been used in commercial grade electronic and white goods. As technologies improve and packaging architectures become more advanced, there are increases in the demands for electronic manufacturing. Understanding the drivers for change in electronic architectures creates an opportunity to explore the materials science of soldering (Evans, 2007).

Packaging architectures refer to assembled leaded devices, printed wiring boards, ball-grid arrays, and chip-scale devices assembled by surface mount processes. The evolution of packaging architectures, shown in Figure 12, has been driven to increase performance and functionality at even smaller product volumes. Pin-in-hole joints enjoyed a monopoly in the industry until surface-mount technology (SMT) was introduced in the mid 1970s. SMT was advantageous as it reduced the size of printed circuit boards and increased the number of lead counts. SMT is still commonly used today due to the ease of automated manufacturing assembly and machine soldering processes that can be employed (Evans, 2007).

Ball-grid arrays (BGAs) were the next step in technological advancement. BGAs are shown in Figure 13 and their smaller counterparts, chip-scale package (CSPs). BGAs are intended to be used in active devices and may also be used for surface-mount applications, allowing all or part of the device footprint to be used for the interconnection pattern (Evans, 2007).

Flip-chips improved upon BGAs by offering superior electrical performance, potentially higher reliability, reduced footprint, and potentially reduced cost depending on the application (Evans, 2007). Flip-chip arrays can be simplified into three basic building blocks: the bumps on the chip, the substrate, and the method of joining the chip on the substrate. Several methods have been used to bond the chip to the substrate including thermocompression, thermosonic bonding, soldering, and adhesive joining (Boustedt, 1998). Flip-chip packaging was developed for mounting a chip directly on a substrate using various interconnection materials. Flip-chip arrays can be utilized in various configurations, which are shown in Figure 14.

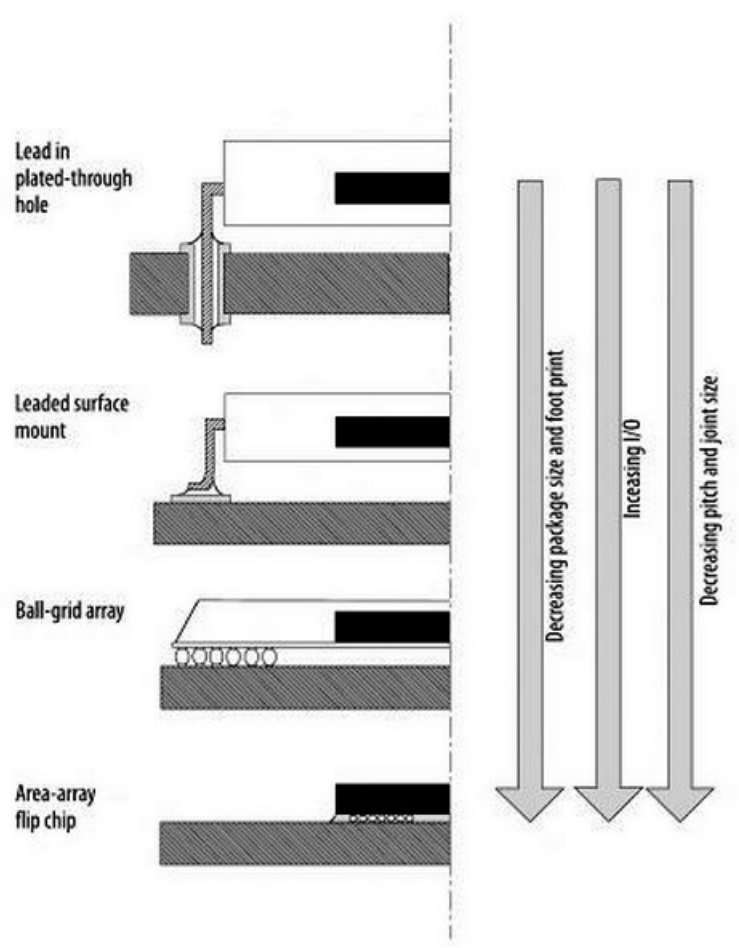

Figure 12: Development of solder joints in relation to packaging architectures (Evans, 2007).

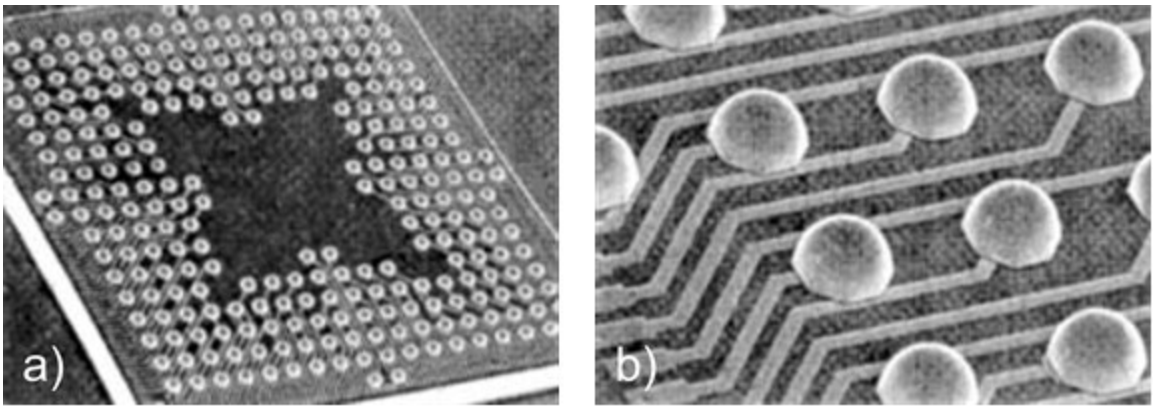

Figure 13: Example of a ball-grid array. a) Low magnification image and b) high magnification image (Evans, 2007).

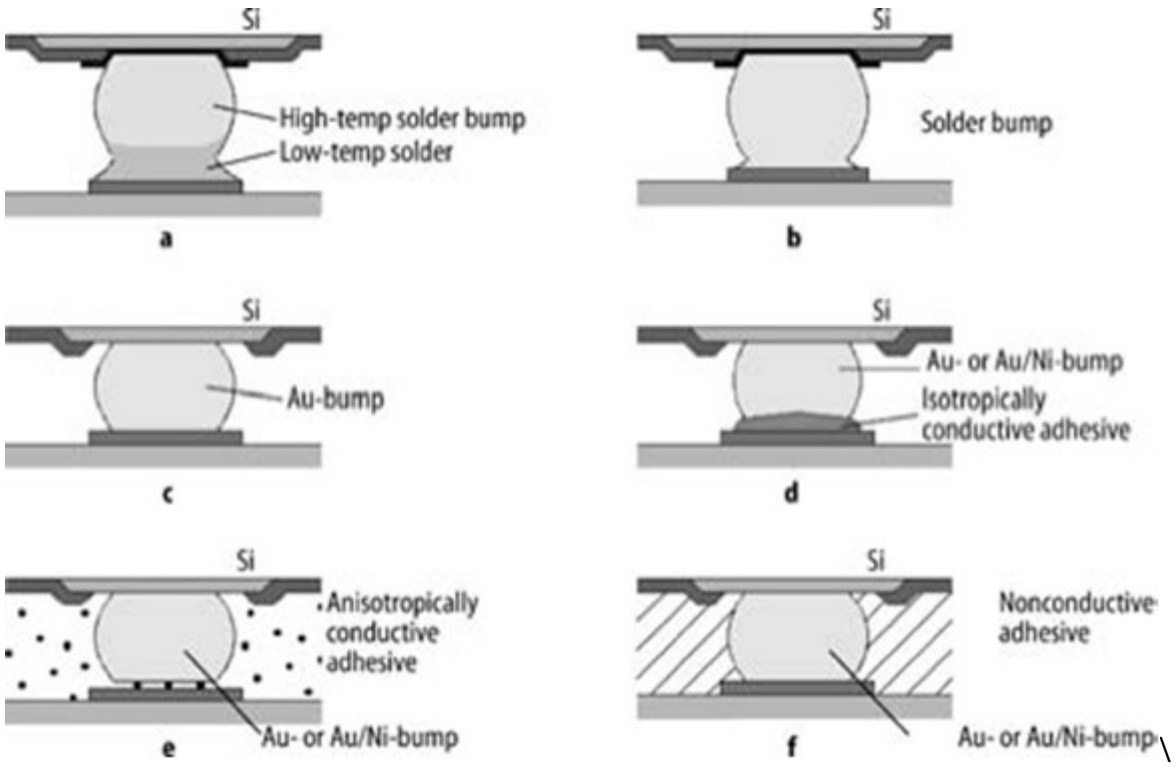

Figure 14: Various types of flip-chip joints (Evans, 2007).

Chapter 3: Experimental Procedures and Analytical Techniques

Electrolyte Preparation

The electrolyte preparation was designed based on a batch process approach. Small quantities of the electroplating electrolytes were prepared to test one variable at a time. This design approach allowed for mass balances to be completed in order to determine the consumption of elements in the electrolyte and to determine the parameters that affected deposit composition and morphology.

Small quantities (35 mL) of the electrolyte were prepared for single use experiments. Initial experiments were conducted with an Sn electrolyte mixed with an Au nano-particle suspension. The electrolyte evolved through the initial results to an Sn electrolyte with the addition of sub-micron Au particles.

Tin Electrolyte

The Sn electrolyte used was composed of one complexing agent, tri-ammonium citrate ($(NH_4)_3HC_6H_5O_7$), and tin chloride ($SnCl_2 \bullet 2H_20$), corresponding to our group's goal of using simple, cost-effective electrodeposition electrolytes (He and Ivey 2008). The particular Sn electrolyte was composed of 75 g/L of $(NH_4)_3HC_6H_5O_7$ and 50 g/L of $SnCl_2 \bullet 2H_20$.

Electrolytes were prepared in 35 mL batches as described in the following procedure. An analytical balance was used to measure 2.625 g of $(NH_4)_3HC_6H_5O_7$, which was then transferred to a 50 mL Erlenmeyer flask along with 35 mL of de-ionized water. A swirling motion was used to dissolve the $(NH_4)_3HC_6H_5O_7$ into the water. After the $(NH_4)_3HC_6H_5O_7$ was completely dissolved, 1.75 g of $SnCl_2 \bullet 2H_20$ was added to the electrolyte. A swirling motion was used to completely dissolve the $SnCl_2 \bullet 2H_20$, resulting in a final Sn electrolyte that was clear and colourless.

Gold Nano-particle Suspension

A stock suspension of Au nano-particles was prepared following the procedure described by McFarland et al. (2004). Initially, an electrolyte containing 1.0 mM $HAuCl_4$ was made by dissolving 0.1 g of the salt into 500 mL of distilled water. A second separate electrolyte containing 38.8 mM sodium citrate ($Na_3C_6H_5O_7$) was then prepared by adding 0.5 g of sodium citrate into 50 mL of distilled water (McFarland et al., 2004). The Au nano-particle suspension was prepared by placing 500 mL of the 1.0 mM $HAuCl_4$ stock electrolyte on a hot plate while a magnetic stir bar agitated the solution. After the solution began to boil, the 38.8 mM sodium citrate solution was slowly added to the $HAuCl_4$ solution using an eyedropper. The solution was maintained at a volume of 500 mL by adding de-ionized water. The Au nano-particle suspension was completed when the solution became deep red in colour. The suspension was then allowed to cool to room temperature before use.

Gold Nano-particle Electrolyte

In order to create Sn-rich, Sn-Au solder films, $SnCl_2 \bullet 2H_20$ and $(NH_4)_3HC_6H_5O_7$ were added directly into the Au nano-particle suspension described in the previous section. However, with the addition of $SnCl_2 \bullet 2H_20$ and $(NH_4)_3HC_6H_5O_7$, the Au nano-particles were no longer stable in solution. The Au nano-particles were only able to remain in suspension (without tin chloride or citrate additions) because the citrate anions covered the surface of the Au nano-particles, as shown schematically in Figure 15. The citrate anions interacted with the Au nano-particles through an adsorption interaction which created an electrostatic repulsion that prevented the Au nano-particles from agglomerating and settling out of electrolyte (McFarland et al., 2004). When a strong electrolyte is added, the citrate layer can be stripped off causing the repulsive force between the particles to be eliminated (McFarland et al., 2004). As there is no longer a repulsive force between the Au particles, they will aggregate. Evidence of this phenomenon occurred when the $SnCl_2 \bullet 2H_20$ and $(NH_4)_3HC_6H_5O_7$ were directly added to the suspension.

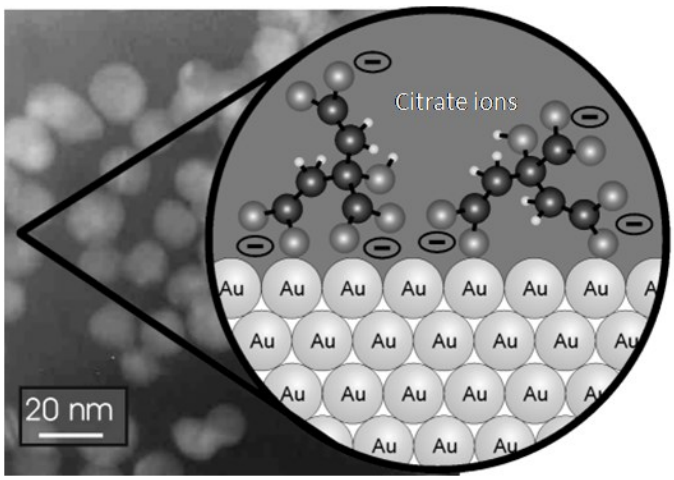

Figure 15: Schematic representation of the citrate layer surrounding the Au nano-particles (McFarland et al., 2004).

Gold Submicron Size Particle Electrolyte

A second electrolyte containing an alternate source of Au was made for comparison with the Au nano-particles. Gold submicron size particles were added directly to the Sn electrolyte (composed of Sn chloride and ammonium acetate). The Au particles were weighed on an analytical scale to achieve predetermined concentrations of 0.5, 0.75, and 1 g/L. Sonic agitation was used prior to electrodeposition to disperse the Au particles in electrolyte.

Electrodeposition Process

Electrodeposition was used to produce Sn-rich, Sn-Au solder films from the batch electrolytes. Films were electrodeposited using 75 g/L of $(NH_4)_3HC_6H_5O_7$ and 50 g/L of $SnCl_2 \bullet 2H_20$ mixed with either an Au nano-particle suspension or Au submicron particles to determine the viability of producing a Sn-rich, Sn-Au solder film. A Dynatronix PR 0.1–10 pulsed current power supply was used for the experiments. Pulse currents were used with an on time of 2 ms and an off time of 8 ms for a period ranging from 30 to 60 minutes. Direct current deposition was used for comparison with pulse current deposition which used an average current density ranging from 5 to 15 mA/cm^2. An electrochemical cell was set up using a 50 mL beaker as a deposition tank shown in Figure 16. Cathode and anode holders were positioned

horizontally and were made from an Al wire with a protective coating. The cathode and anode holders were placed approximately 1 cm apart. Silicon wafers coated with Ti/Au and Ti/Pt were used for the cathodes and anodes, respectively. Ti/Pt wafers were also used as cathodes in some cases. The Au and Pt layers were 500 nm in thickness while the Ti layer was 25 nm thick, and the plating area was set to 0.64 cm^2 using a protective lacquer. De-ionized water was used to clean each sample before and after deposition.

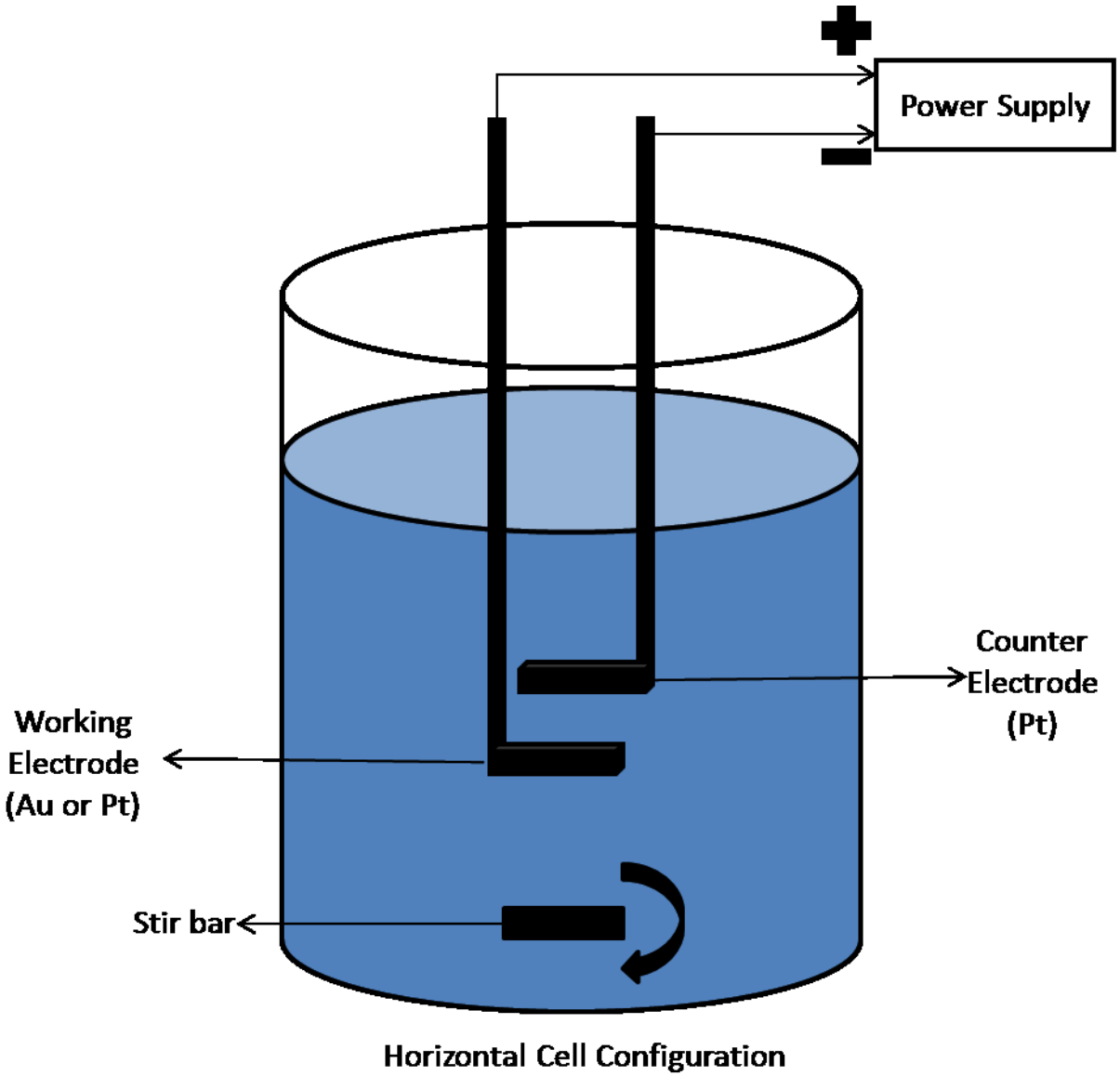

Figure 16: Schematic of the electrochemical cell.

Analytical Techniques

Sample Preparation for Scanning Electron Microscopy (SEM)

Deposits created using the electrodeposition process were prepared for inspection of their morphology and composition. Plan view and cross-sections of the deposits were prepared for analysis. Samples were initially cleaved to create two samples of a single deposit for analysis. One sample was used for plan-view analysis to determine deposit composition and morphology, while the other half was mounted in an epoxy mold for cross-sectional analysis. Cross-sectional samples were prepared using 320 and 600 grit SiC paper and a 0.05 μm alumina suspension to remove any cleaving artifacts. Copper tape was used to ground the samples and to prevent charging effects during SEM annalysis.

Scanning Electron Microscopy (SEM)

A scanning electron microscope has two major components: the electron column and the control console. The electron column is composed of an electron gun and two or more lenses (Goldstein et al., 2003). The electron gun can generate and accelerate electrons with an energy range of 0.1–30 keV producing a spot size of less than 10 nm, which interacts with the specimen to a depth of approximately 1 μm (Goldstein et al., 2003). The lenses influence the path of the highly excited electrons traveling down the electron column. A control console consists of a viewing screen and controls used to adjust the electron beam, lenses, and image quality.

A Hitachi S2700 SEM was used to examine the electrodeposited samples. Images of the surfaces (i.e., plan-view samples) and cross sections were taken. Area and point composition analyses using energy dispersive x-ray spectroscopy (EDS) were also conducted. The following sections describe the procedure taken to obtain secondary electron (SE) images, backscattered electron (BSE) images, and EDS analysis.

Secondary Electron (SE) and Backscattered Electron (BSE) Imaging

The Hitachi S2700 SEM was equipped with a positively biased Everhart-Thornley (E-T) detector and a GW Electronics System was used to collect SE and BSE, respectively, for imaging. The SEs and BSEs have different energies and are produced via different mechanisms. Different information can be extracted by analyzing both SE and BSE images. SE images are

susceptible to changes in topography. BSE images are primarily dependent on the atomic number of the elements present in the sample and create contrast within the image. The E-T detector was used to obtain SE images of both plan-view and cross-sectional samples. The GW Electronics System is a solid-state detector divided into four quadrants to collect BSEs for imaging.

Energy Dispersive X-Ray Spectroscopy (EDS)

An x-ray detector attached to the Hitachi S2700 SEM was used to detect x-rays for EDS analysis. The specific x-ray detector used was a Prism Intrinsic Germanium (IG) semiconductor. An accelerating voltage of 20 kV at a working distance of 17 mm was utilized and the probe current was increased to obtain a count rate ranging from 2000–3500 counts/seconds. The working distance and aperture size were set to 17 mm and 50 μm, respectively. The x-ray collection time was set to 90 seconds.

Pure Au and Sn standards were used for quantitative analysis to determine the composition of the electroplated films. To determine the overall composition for each sample, three areas 200 μm by 200 μm were selected and analyzed. The average composition was reported in the results along with one standard deviation. In some cases, point analysis was done.

Secondary Analytical Techniques

Secondary analytical techniques were used to confirm the chemical composition and size of the nano-Au particles and submicron Au particles. This section provides brief descriptions of Zeta potential, x-ray photoelectron spectroscopy (XPS), and transmission electron microscopy (TEM) analysis.

Zeta Potential

Zeta potential was used as a verification technique to confirm the size of the Au nano-particles in suspension. The majority of the macroscopic materials or particulates that come into contact with a liquid will acquire an electronic charge on their surfaces. Zeta potential can be used as an indicator of this charge. Moreover, zeta potential can be used to predict and control the stability of colloidal suspensions/emulsions or as a controlling parameter in processes such as

adhesion, surface coating, filtration, lubrication, and corrosion. A ZetaPlus zeta potential analyzer from Brookhaven Instruments Corp. was used to measure the diameter of the Au nano-particles. The ZetaPlus system used software that measured the particle size by dynamic light scattering (www.brookhaven.co.uk).

X-ray Photoelectron Spectroscopy (XPS)

XPS is primarily a surface analysis technique that gathers information 0.5–2.5 nm from the surface (Goldstein et al., 2003). In XPS, electrons are ejected from their localized core levels by photon energy. A plot of photoelectron flux against measured kinetic energy can be created, revealing a series of peaks corresponding to the orbital structure of the atom (Goldstein et al., 2003). XPS was carried out with a Kratos AXIS 165 XPS system using a monochromatic Al Kα source and a current of 15 mA.

Transmission Electron Microscopy (TEM)

Transmission electron microscopy was used as a secondary verification method for the nano-Au particles. TEM samples were prepared by placing droplets of the nano-Au particle suspension onto a carbon grid and allowing the water to evaporate. TEM images are produced using a beam of highly energized electrons that are guided by a series of electromagnetic lenses under a vacuum. The beam of electrons then passes through the sample creating an image on a fluorescent screen. Electron diffraction patterns and bright field images of the nano-Au particles were taken using a JEOL-2010 TEM.

Chapter 4: Codeposition with Au Nano-Particles

Au nano-particle suspension. This approach was investigated first in an effort to determine some of the characteristics of the suspension. The initial concern when using an Au nano-particle suspension was the actual size of the particles and whether the suspension was sustainable. Sizing of the Au nano-particles was completed using two different methods—the ZetaPlus analyzer and TEM. These methods verified that the particle size of the Au nano-particles prior to attempting codeposition.

Nano-Au particle size determination. Particle size determination was initially completed using ZetaPlus techniques. The sedimentation method employed here resulted in a statistical distribution (Figure 16) indicating the mean diameter of the Au nano-particles was 100 nm. This mean diameter was greater by about an order of magnitude than expected. Thus, further investigation was required to confirm the diameter of the Au nano-particles prior to deposition experiments. TEM techniques were used as a second method of confirming the size of the Au nano-particles and their chemical makeup. TEM analysis, shown in Figure 17, revealed that the Au nano-particles were approximately 10 nm in diameter. Agglomeration and fused particles were also observed in the TEM images, accounting for the larger Au particle diameter determined using the ZetaPlus method. Electron diffraction patterns were obtained and confirmed the crystal structure of the particles. The ring pattern shown in Figure 17a was taken from the region shown in Figure 17b. The (111), (200), (220), and (311) planes for Au were confirmed. No other phases were detected.

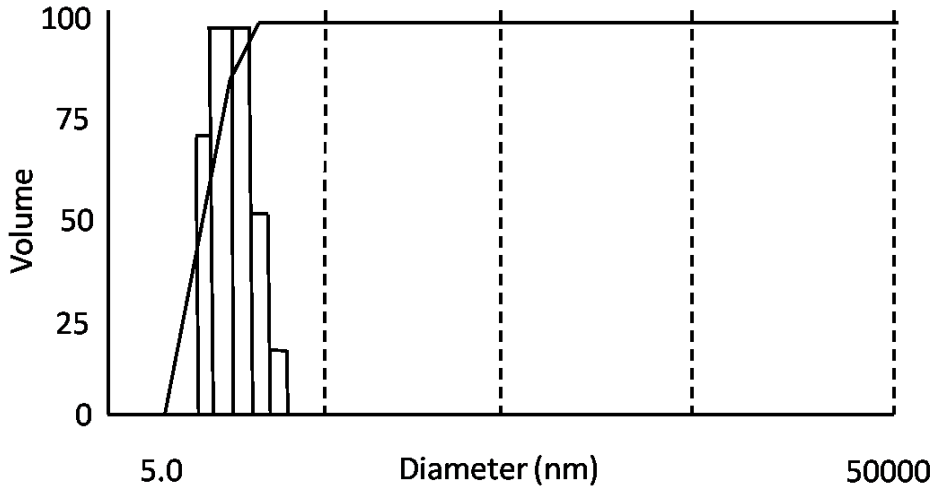

Figure 17: Distribution of Au nano-particle diameters using ZetaPlus sizing software. (The x-axis is displayed on a log scale.)

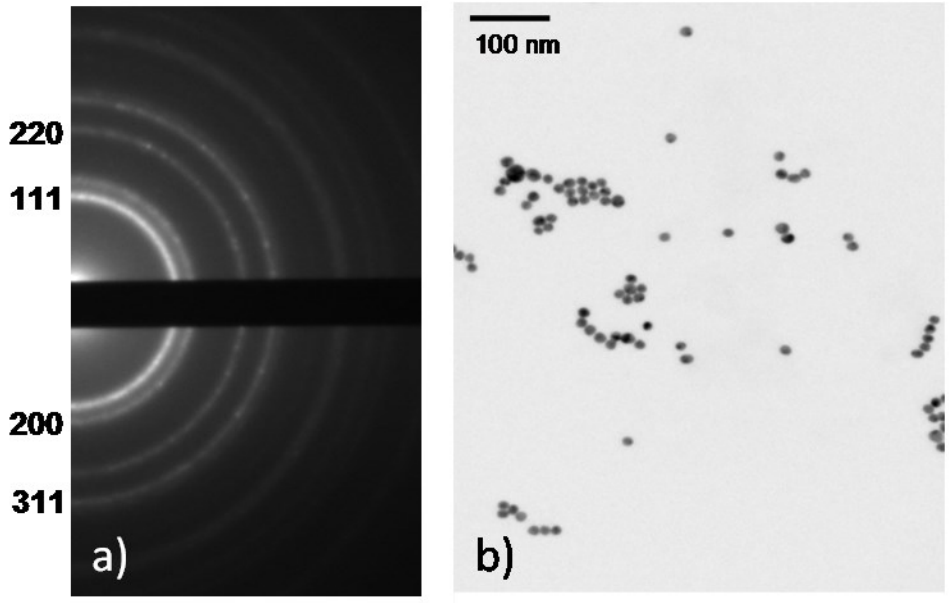

Figure 18: Indexed electron diffraction pattern (left) and TEM bright field image of Au nano-particles (right).

Electrodeposition using Au nano-particles. This process was initially completed on a Pt-metalized substrate using a Sn electrolyte, containing 75 g/L $(NH_4)_3HC_6H_5O_7$ and 50 g/L $SnCl_2 \bullet 2H_20$ mixed into 30 mL of the Au nano partical suspension, at an average current density of 7.5 mA/cm^2 and a duty cycle of 20%. The first attempts at deposition resulted in a rough surface. The low magnification plan-view and high magnification cross-sectional view in Figures 18a and 18b, respectively, show a non-uniform Sn-Au deposit. EDS analysis of the film, depicted in Figure 19, indicate a deposit composition of 99.2 wt% Sn and 0.8 wt% Au. A second deposit using the same electrolyte chemistry was allowed to equilibrate, causing the Au nano-particles to completely settle out of the electrolyte. It was then sonically agitated to disperse the Au nano-particles before deposition, which was completed under the same conditions as the first attempt. The resulting deposit (Figure 20) shows a relatively smooth surface and a uniform deposit. Upon closer examination of the deposit, it was difficult to confirm the presence of Au nano-particles. EDS analysis, shown in Figure 21, indicates that the deposit contained 1 wt% Au.

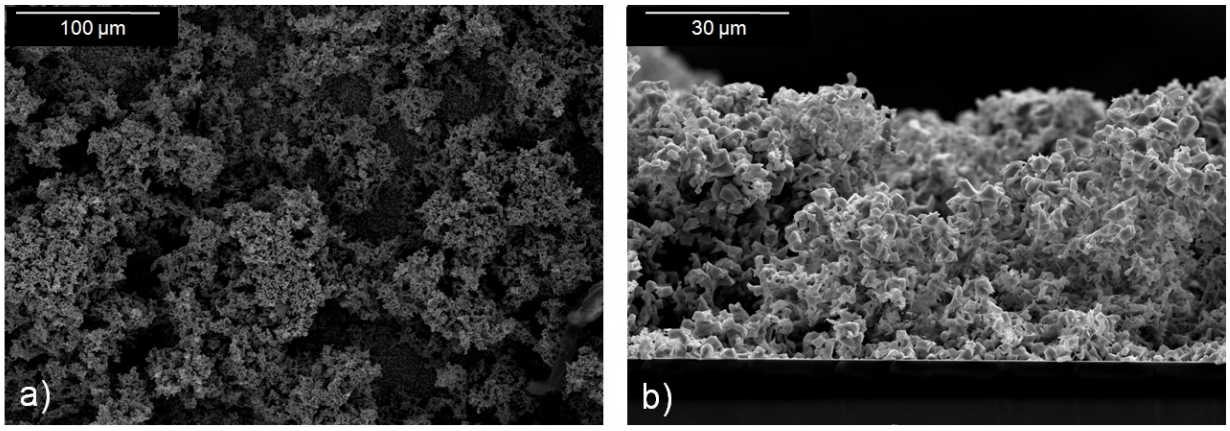

Figure 19: SEM SE images of a deposit on a Pt metallized substrate produced from a fresh electrolyte mixed with the Au nano-particle suspension. Image (a) is a low-magnification plan-view image, whereas image (b) is a higher magnification cross-sectional view.

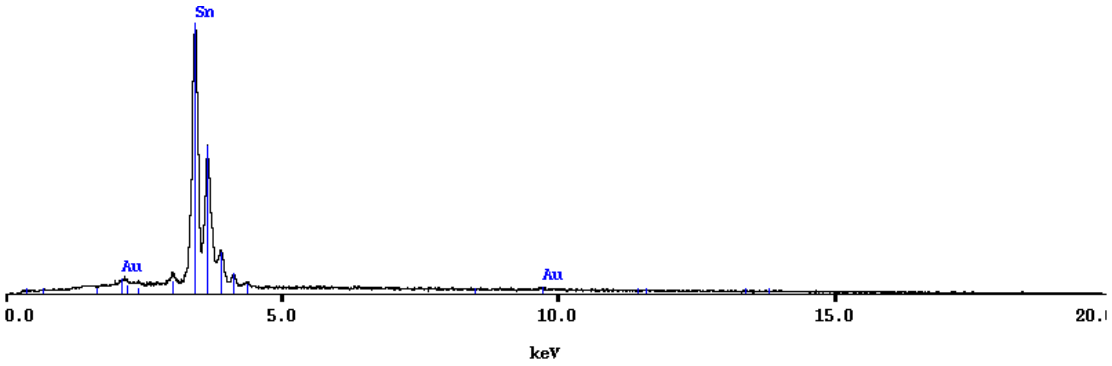

Figure 20: EDS spectrum from the deposit shown in Figure 18.

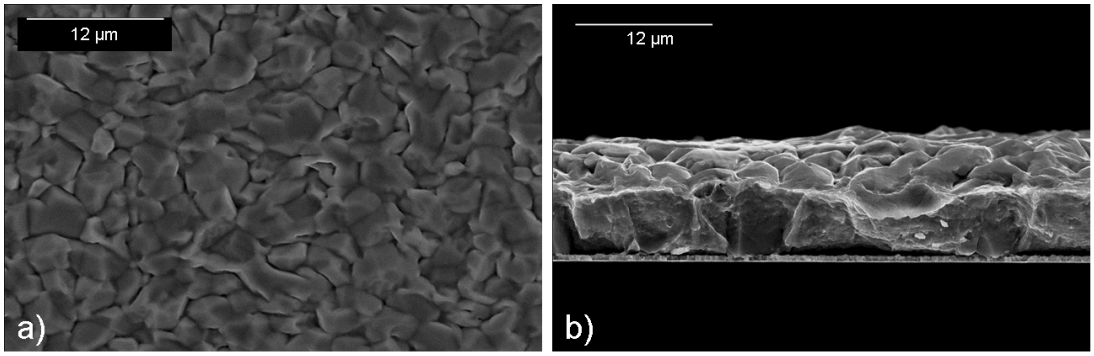

Figure 21: SEM SE images of a deposit produced using an aged electrolyte mixed with the Au nano-particle suspension. Images (a) and (b) are plan-view and cross-sectional view images, respectively.

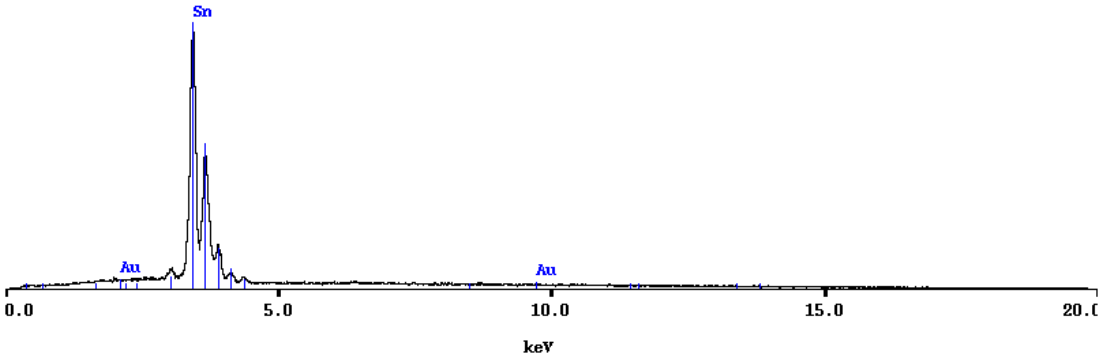

Figure 22: EDS spectrum from the deposit shown in Figure 20.

There was evidence that Au nano-particles were settling during deposition. It was also believed that agitation removed the Au particles from the surface of the deposit before they could become incorporated into the deposit. In order to test this hypothesis, an additional deposit was completed using an aged nano-Au electrolyte without the use of magnetic stirring (Figure 22). The plan-view image in Figure 22a shows a similar morphology to Figure 20, where the electrolyte was stirred throughout the plating process. Without magnetic stirring during deposition, more Au nano-particles are evident in the deposit. However, the nano-Au particle agglomerates appear to be only on the surface of the deposit (Figure 22a). Nano-Au clusters were confirmed from EDS analysis (Figure 3.8), which indicated a maximum overall Au composition of 1 wt% Au. The EDS analysis and cross-sectional image in Figure 23 confirm that the Au nano-particles are not incorporated within the bulk of the deposit.

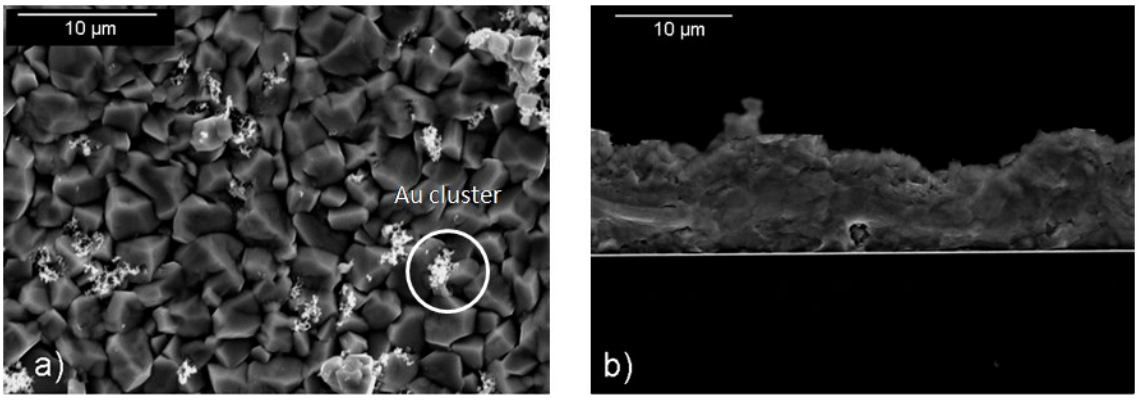

Figure 23: SEM SE images of deposit fabricated using an aged Sn electrolyte mixed with the Au nano-particle suspension, without magnetic stirring. Images (a) and (b) are plan-view and cross-sectional view images, respectively.

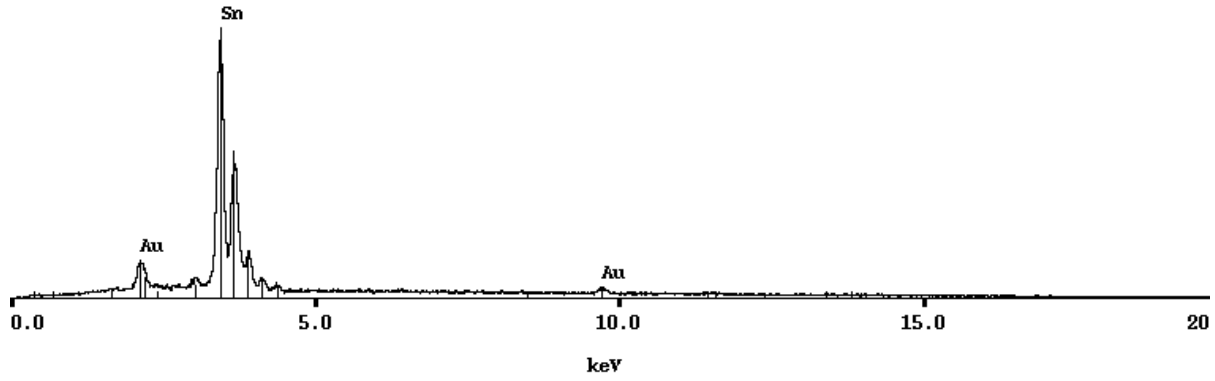

Figure 24: EDS spectrum from a Au nano-particle cluster in Figure 22a (circled region).

As indicated by the initial results, the original electrolyte created by adding tin chloride and tri-ammonium citrate directly to the Au nano-particle suspension was not a viable option for producing Sn-rich, Sn-Au solder deposits. In an attempt to incorporate the Au nano-particles into the film, the electrolyte chemistry (i.e., the amount of Au and Sn in the electrolyte) was adjusted.

Adjusting the electrolyte chemistry may make it possible to increase the amount of Au incorporated into the deposits. Therefore, the electrolyte chemistries were changed in two different ways to achieve a deposit with a higher Au content. In the first scenario, the concentration of Au nano-particles was increased in the electrolyte. Water was evaporated from the Au nano-particle suspension in order to achieve the required amount of Au in the electrolyte before adding the tin chloride and tri-ammonium citrate. The second scenario involved reducing the amount of tri-ammonium citrate and tin chloride that was added directly to the standard nano-Au particle suspension.

The first scenario resulted in the deposits shown in Figure 24; two different Au concentrations were utilized, Au:Sn ratios of 1:125 and 1:166 in the electrolyte. For the second scenario, the amount of tin chloride and ammonium citrate were reduced (to give Au:Sn ratios in the electrolyte of 1:125 and 1:50). The deposits are shown in Figures 25a-d. Both scenarios resulted in an increase in the amount of Au nano-particles incorporated into the deposit, ranging from 1 wt% to 5 wt%. However, the increase in incorporated Au nano-particles resulted in non-uniform deposits. When tin chloride was added to the Au nano-particle suspension, the Au

particles agglomerated instantly and settled to the bottom. This agglomeration indicates that the electrolyte does not contain the appropriate amount of citrate to suspend the Au nano-particles and to complex the tin in electrolyte. Moreover, the tin chloride interacted and removed the citrate layer around the Au nano-particles causing agglomeration of the Au nano-particles. A deposit using a current density of 7.5 mA/cm^2 and a duty cycle of 20% was employed after the electrolyte underwent sonic agitation to disperse the Au particles. The resulting electrolyte created a deposit that had poor morphology and was composed of loosely deposited Sn islands (Figure 26).

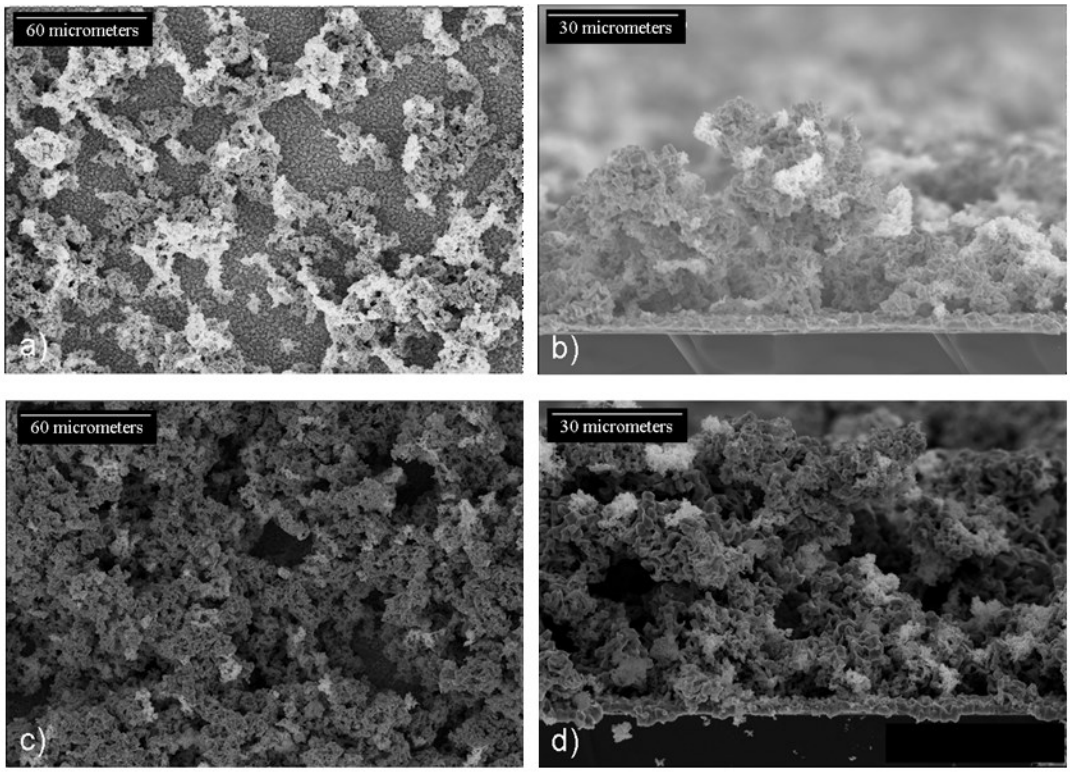

Figure 25: SEM BSE images of deposits fabricated from an electrolyte with an increased amount of Au nano-particles. Images (a) and (b) are a plan-view and cross-sectional view, respectively, of a deposit from an electrolyte with an Au to Sn ratio of 1:125. Images (c) and (d) are a plan-view and cross-sectional view, respectively, of a deposit from an electrolyte with an Au to Sn ratio of 1:166.

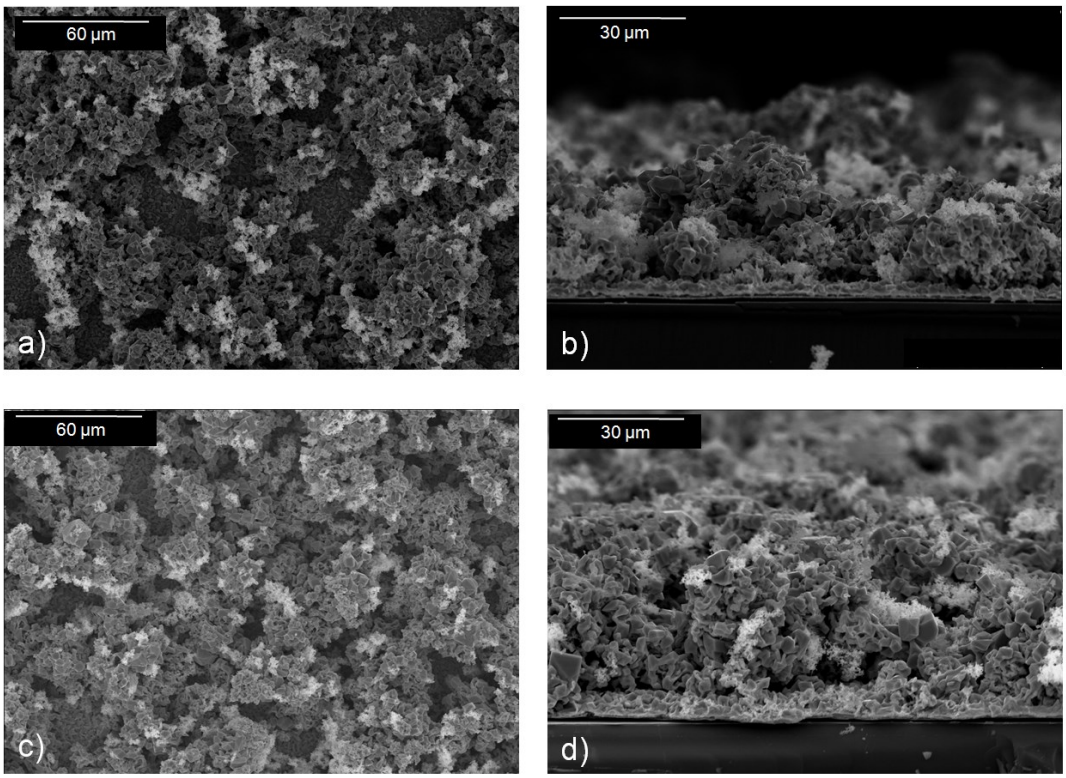

Figure 26: SEM BSE images of deposits fabricated using a reduction of Sn in the electrolyte. Images (a) and (b) are a plan-view and cross-sectional view, respectively of a deposit from an electrolyte with an Au to Sn ratio of 1:125. Images (c) and (d) are a plan-view and cross-sectional view, respectively, of a deposit from an electrolyte with an Au to Sn ratio of 1:50.

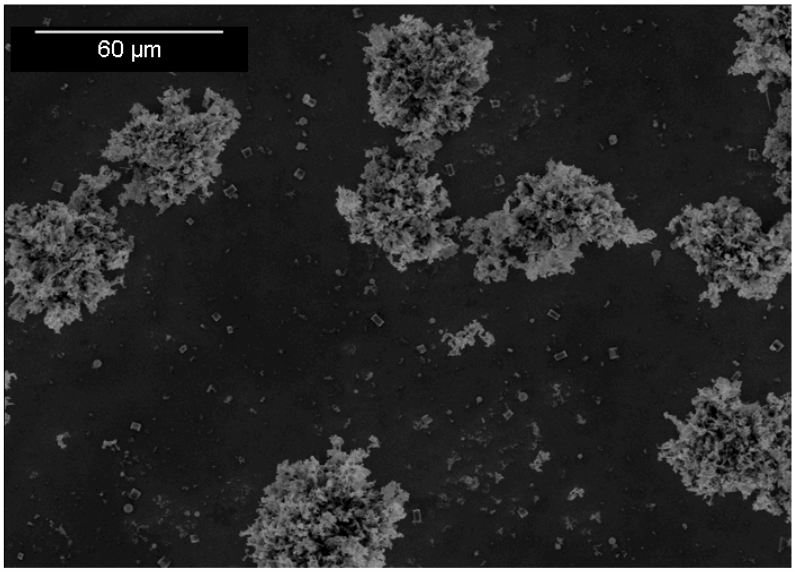

Figure 27: SEM SE plan-view image of a deposit from an electrolyte without the addition of tri-ammonium citrate.

Adjusting the electrolyte chemistry, by varying the amount of Au nano-particles or the amount of the tin electrolyte, increased the amount of Au present in the deposit at the cost of deposit morphology. In an attempt to improve the morphology and to increase the Au content, a Sn electrolyte was produced using sodium citrate rather than tri-ammonium citrate. Sodium citrate is the same additive used in the formation of the nano-Au particle suspension. The change from tri-ammonium citrate to sodium citrate caused the Au nano-particles to settle out of the suspension and decreased the stability of the Sn electrolyte. Deposits using a current density of 7.5 mA/cm^2 were fabricated using the electrolyte containing sodium citrate; a similar porous Sn morphology seen in previous deposits was obtained (Figure 27). However, unlike other altered electrolytes, no Au was deposited.

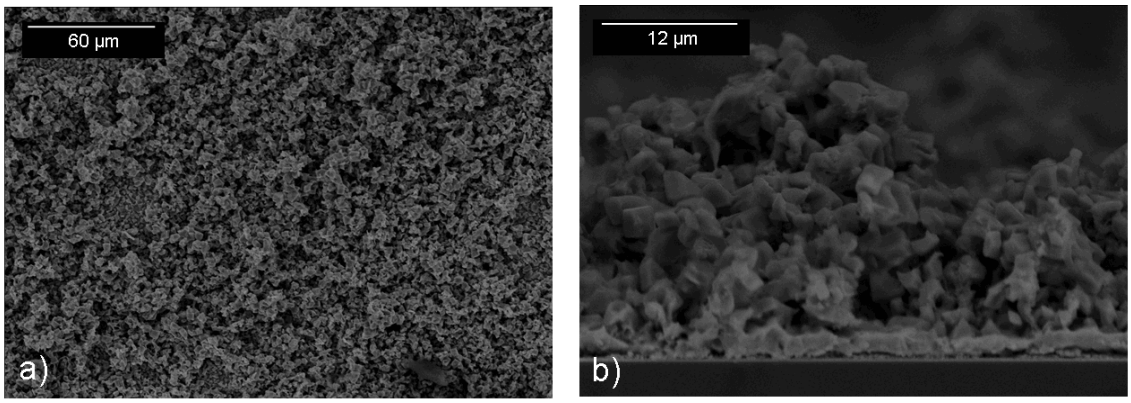

Figure 28: SEM SE images of a deposit using an electrolyte containing sodium citrate in place of ammonium citrate. Images (a) and (b) are a plan-view and cross-sectional view, respectively.

A non-uniform and porous Sn morphology tends to be the common outcome when using a nano-Au suspension mixed with the Sn electrolyte, containing tin chloride and ammonium citrate. Three additives were chosen in an attempt to improve the Sn deposit morphology: sodium metaphosphate, dextrin, and a leveler composed of gelatin and naphthol. These additives were added to three separate electrolytes and the quantity of each additive is summarized in Table 6.

Table 6 Quantity of Additives Added to the Electrolyte

Additive	Amount Added
Sodium Metaphosphate	0.1 g/L
Dextrin	0.1 g/L
Leveler (Gelatin and Naphthol)	17 mL

Sodium metaphosphate and dextrin improved the morphology of the deposits, producing smoother and more uniform deposits that are shown in Figure 28. The leveler improved the morphology of the deposit; however, larger islands of Sn can be seen growing on the surface of the deposits (Figure 28). EDS analysis of the deposits indicated that Au nano-particles were not incorporated into the deposits.

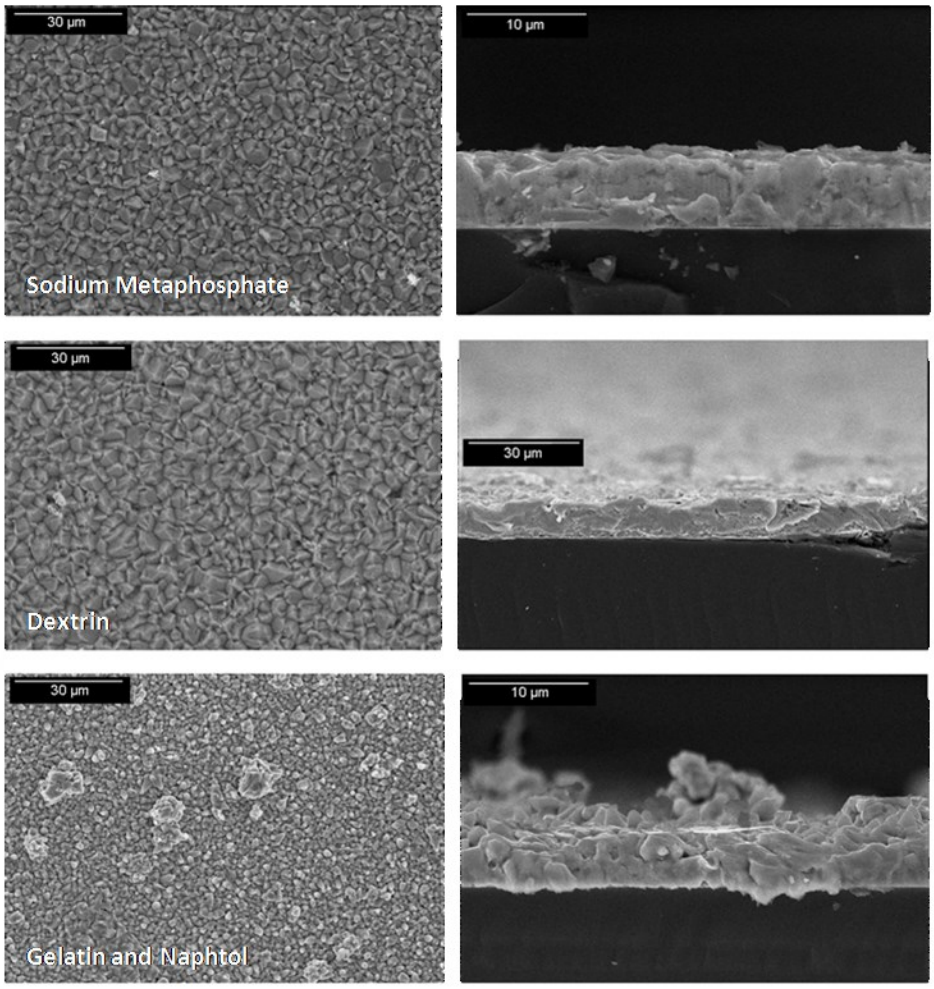

Figure 29: SEM BSE images of deposit morphology improvements with additives to the nano-Au particle containing electrolyte.

For samples with an increased amount of Au nano-particles in the electrolyte, sodium metaphosphate and dextrin improved the morphology of the film. However, EDS analysis

indicated the deposits were comprised of only Sn. The addition of a leveler to the electrolytes, with an increased quantity of Au nano-particles, yielded a different result than the sodium metaphosphate and dextrin. The addition of a leveler improved the morphology of the Sn layers deposited, but also acted like a "glue" causing the Au nano-particles to agglomerate and deposit on the surface on the deposits, as shown in Figure 29. This agglomeration of Au nano-particles on the surface is a negative side effect of the leveler, leading to an uneven distribution of Au nano-particles in the deposited Sn layers.

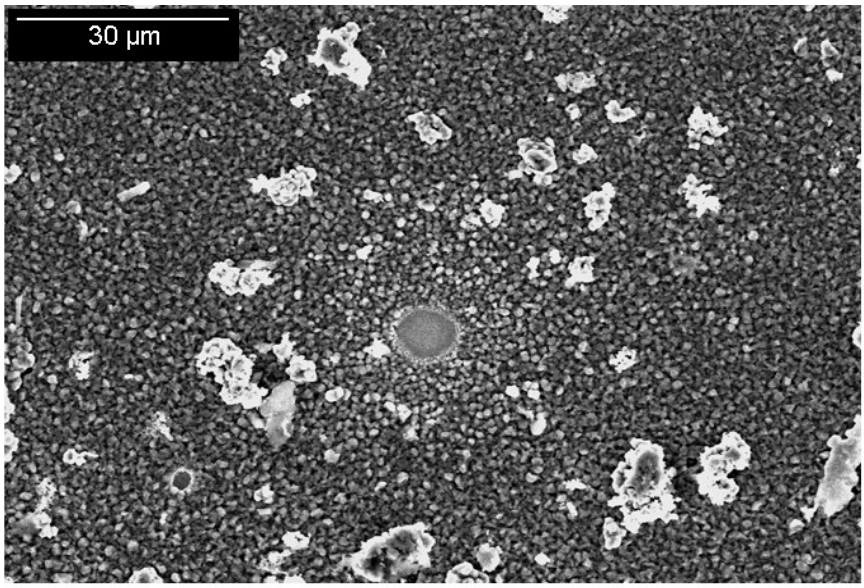

Figure 30: SEM BSE image of a deposited fabricated from an electrolyte containing a leveler. Agglomerated Au nano-particles are present on the surface.

Summary. Codeposition using Au nano-particles to produce a viable Sn-rich, Sn-Au solder deposit is a challenging process. Direct addition of tri-ammonium citrate and tin chloride to an Au nano-particle suspension produces a relatively smooth Sn layer. The small size of the Au nano-particles and the concentration difference between the Sn and Au components in the electrolyte make it difficult to codeposit Au nano-particles along with the Sn. Changes to the electrolyte (i.e., the concentration of nano-Au and Sn) can increase the amount of Au nano-particles deposited, at the expense of deposit morphology. Additives can improve deposit

morphology, but inevitably prevent incorporation of Au nano-particles into the deposit. Since the relationship between Sn deposit morphology and incorporation of Au nano-particles is complex, a decision was made to develop a different electrolyte. Instead of an Au nano-particle suspension as the Au source, submicron Au particles were added directly to the Sn electrolyte. The direct addition of submicron Au particles simplifies the electrochemistry, producing a simple electrodeposition procedure that enables the goal of producing simple and cost-effective solder films. This work will be presented in the next chapter.

Chapter 5: Codeposition using Sub-Micron Au Particles

The next stage of the process of developing a simplified Sn-Au electrodeposition process, to produce a Sn-rich, Sn-Au deposit, involved an Sn electrolyte with submicron Au particles added,. The reason for switching the source of Au within the electrolyte was to limit the large number of variables created by using a Au nano-particle suspension as the Au source. Submicron Au particles pose some advantages over the Au nano-particle suspension, as discussed in this chapter. To simplify the electrodeposition process, submicron Au particles were directly added to the Sn electrolyte.

Submicron Au particles. The size of these particles was verified using SEM analysis (Figure 30a), which revealed that the particles ranged from 0.5 to 1 μm in diameter. EDS analysis (shown in Figure 30b) indicated that the Au particles were pure. Additionally, XPS analysis was done specifically to determine if the submicron Au particles were coated. XPS was utilized as an additional characterization method, as low atomic number elements are difficult to detect by EDS analysis. The XPS results shown in Figure 31 show the presence of C 1s, O 1s and N 1s peaks. The presence of nitrogen and oxygen, in particular, is an indication that there is an organic coating on the Au particles. The intensities of the N 1s and O 1s peaks are not typical of atmospheric contamination, although the carbon tape used to secure the submicron Au particles could be responsible, in part at least, for the C 1s peak. The results show that an organic coating was present on the submicron Au particles, which was later confirmed by Sigma Aldrich. The specific coating could not be identified for proprietary reasons.

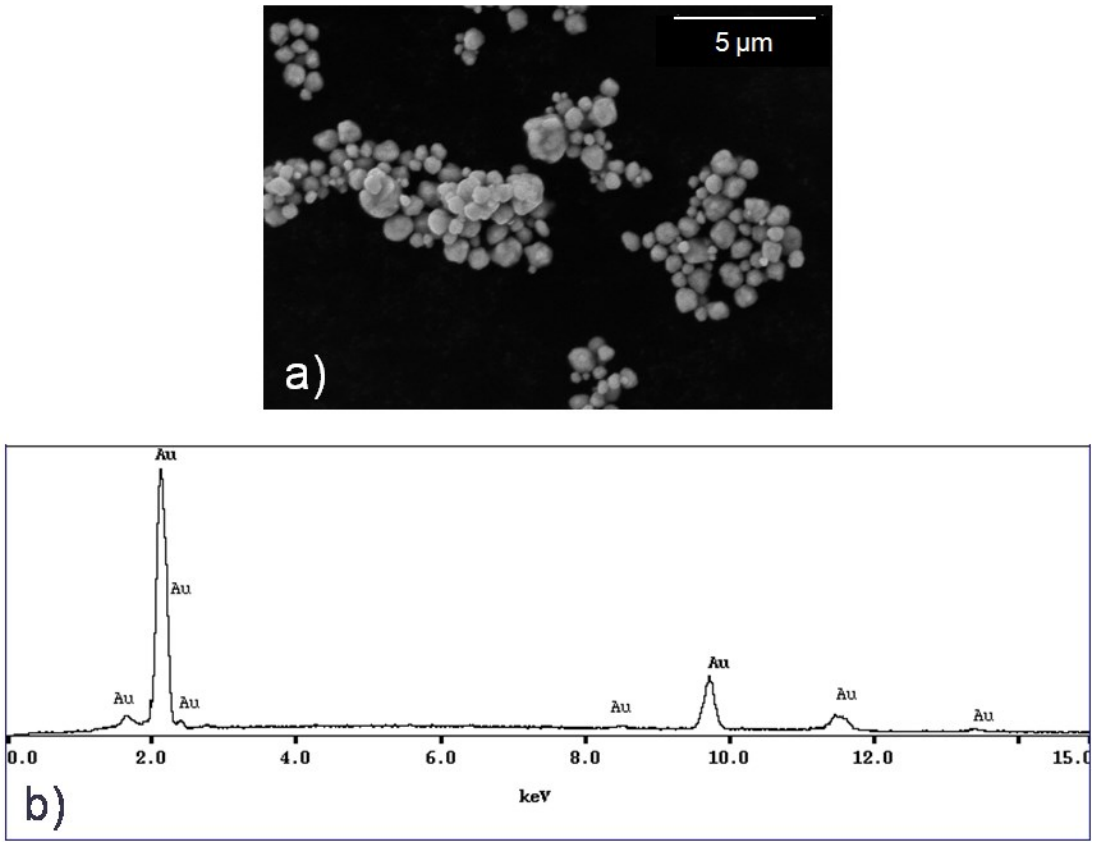

Figure 31: a) SEM SE image of submicron Au particles. b) Corresponding EDS spectrum from the same Au particles.

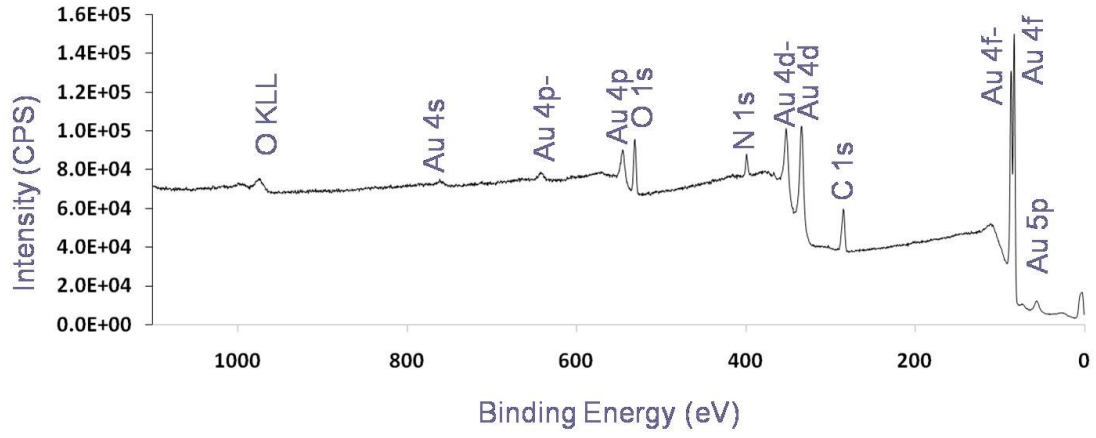

Figure 32: XPS spectrum from the submicron Au particles.

Electrodeposition using submicron Au particles. This process was initially completed to explore the effects of particle additions to the Sn electrolyte containing 75 g/L $(NH_4)_3HC_6H_5O_7$ and 50 g/L $SnCl_2 \bullet 2H_20$. A sample that was electrodeposited with the Sn electrolyte was compared with a sample that was electrodeposited from the Sn electrolyte containing a submicron Au particle concentration of 1 g/L. The submicron Au particles present in the Sn electrolyte bath did not affect the morphology of the Sn deposit, as shown in Figure 32. However, the deposition rate decreased for deposits containing the Au particles. A typical deposition rate for the Sn electrolyte is ~20 μm/h at a current density of 10 mA/cm^2, while the deposition rate at the same current density for the electrolyte containing the Au particles is ~15 μm/h.

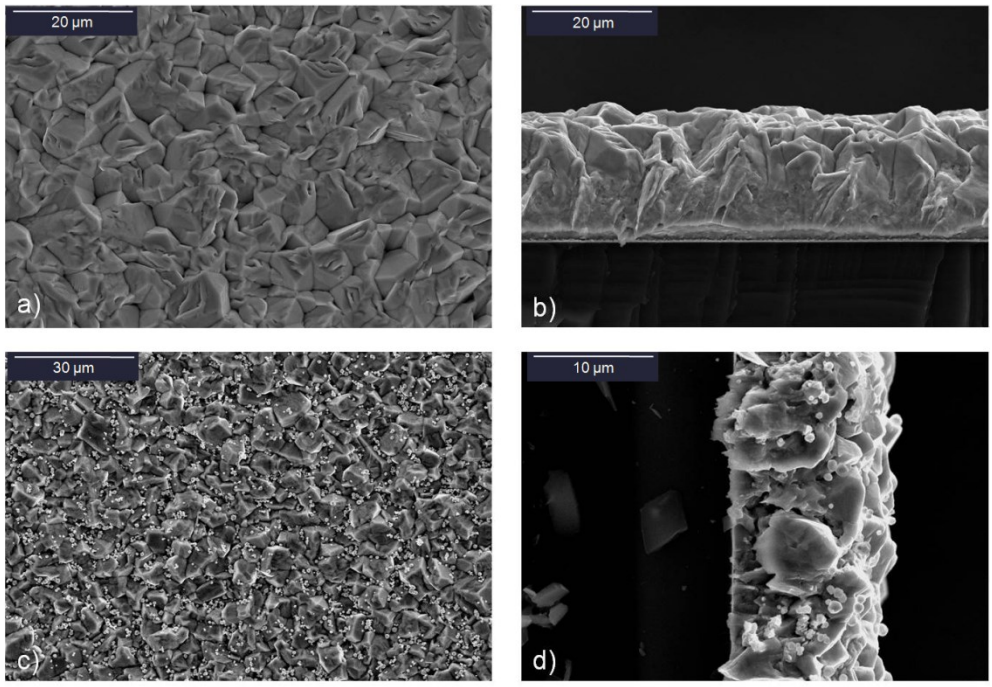

Figure 33: SEM SE images comparing deposits from Sn electrolytes with and without Au particles. Images (a) and (b) are a plan-view and a cross-sectional view, respectively, of a deposit from an Sn electrolyte. Images (c) and (d) are a plan-view and a cross-sectional view, respectively, of a deposit from a Sn electrolyte with direct addition of submicron Au particles (1 g/L).

The next approach was to determine effect of current density on the morphology and composition of the solder film. Pulse current and direct current were used to determine the effects of current density. To ensure that current density was the only factor being explored, the experimental setup was fixed and a fresh electrolyte was used for each experiment. Fresh electrolytes were used to eliminate any changes in deposit composition that may arise from consumption of submicron Au particles during the deposition process. The Au particle loading was fixed at 1 g/L. The results of adjusting current density are shown in Figure 33. The organic coating did not affect the deposition of submicron Au particles when the current density was changed. As the current density was increased from 5 to 15 mA/cm^2, the deposit composition remained constant at around 5–6 wt%, as shown in Figure 33. Moreover, the deposit morphology over the range of 5–10 mA/cm^2 remained smooth.

Direct current deposition, shown in Figure 34, was also used to investigate the effect on the composition of the deposit. The continual buildup of the Sn layer or increase in surface roughness may incorporate more Au particles by trapping them during deposition. However, EDS analysis of the samples indicates the composition ranged from 4.5–6 wt% Au, which is similar to the deposits created using pulse deposition. Thus, the incorporation of Au particles into the deposit is not influenced by the deposition process or current density used.

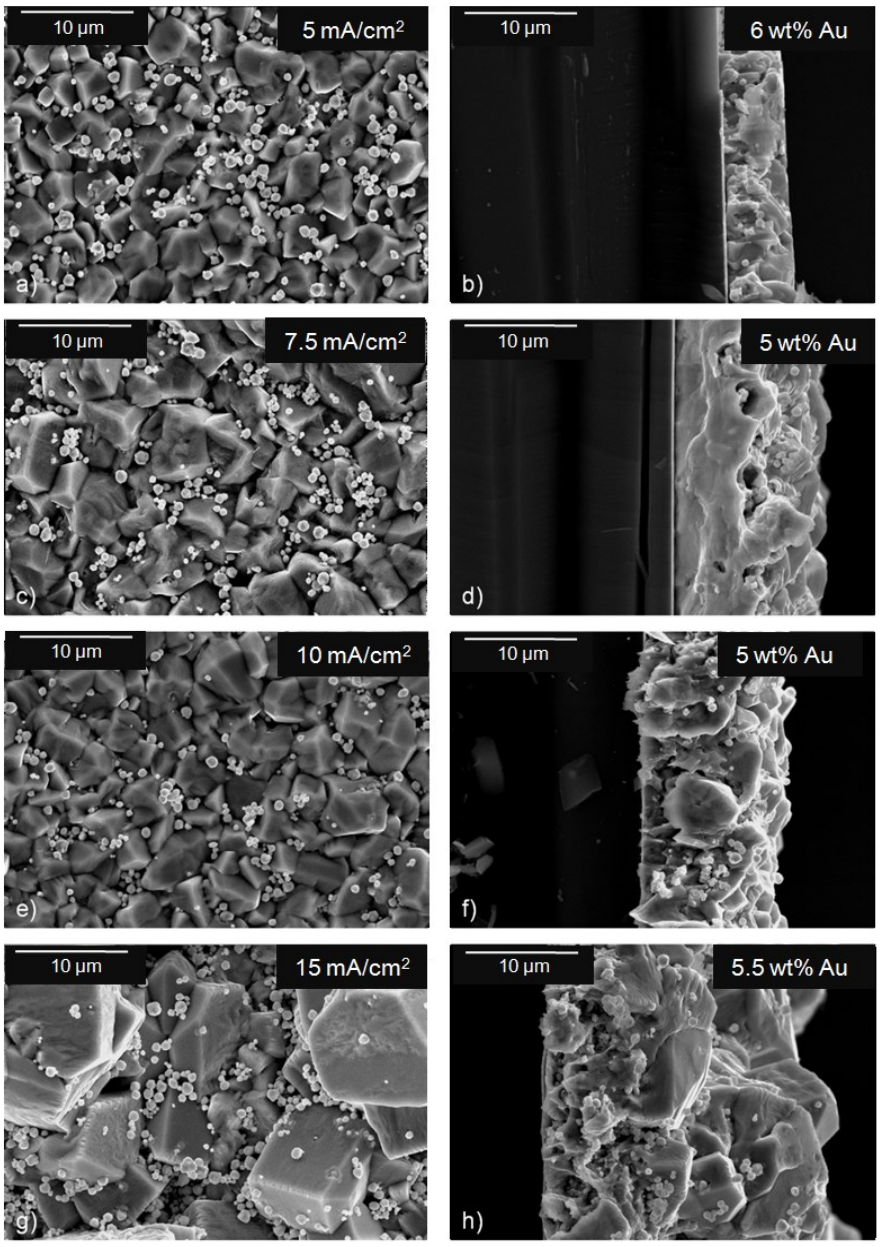

Figure 34: SEM SE images showing the effects of current density on Au incorporation using a Sn electrolyte with 1 g/L submicron Au particle loading. Images (a) and (b) are a plan-view and cross-sectional view, respectively, of a sample fabricated using a current density of 5 mA/cm^2. Images (c) and (d) are a plan-view and cross-sectional view, respectively of a sample fabricated using a current density of 7.5 mA/cm^2. Images (e) and (f) are a plan-view and cross-sectional view, respectively, of a sample fabricated using a current density of 10 mA/cm^2. Images (g) and (h) are a plan-view and cross-sectional view, respectively, of a sample fabricated using a current density of 15 mA/cm^2.

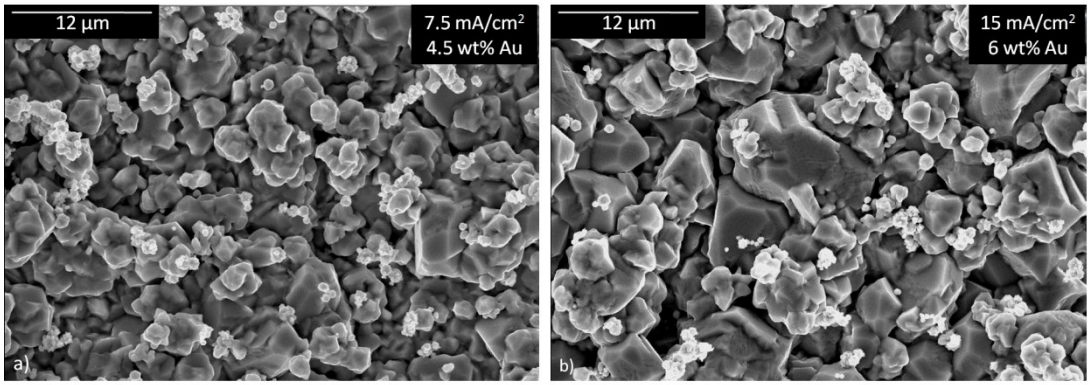

Figure 35: SEM SE images for direct current deposition using a Sn electrolyte with 1 g/L submicron Au particle loading. Image (a) is a plan-view of a sample created using a current density of 7.5 mA/cm^2. Image (b) is a plan-view of a sample created using a current density of 15 mA/cm^2.

Varying the concentration of the submicron Au particles can customize the electroplating electrolyte for various applications. In order to determine the functionality of the submicron Au particles, particle loading in the electrolyte was examined. Parameters of interest include variation in film composition and reproducibility with multiple depositions from the same electrolyte.

Particle loadings of 0.5, 0.75, and 1 g/L, at two different current densities, were investigated. The effect of particle loading is summarized in Table 7. The Au composition in the deposits increased as particle loading increased from 0.5 g/L to 0.75 g/L, for a current density of 7.5 mA/cm^2, and then leveled off. For a current density of 10 mA/cm^2, the Au composition increased as the particle loading increased. In general, the Au composition in the deposits was higher for the higher current density (10 mA/cm^2), at the same particle loading. The exception was the samples deposited from an electrolyte with a particle loading of 0.75 g/L; a higher current density gave a lower Au composition in the deposit.

Table 7 Summary of Particle Loading Effects on Deposit Composition

Particle Loading		7.5 mA/cm^2	10 mA/cm^2
0.5 g/L Au	Average Composition	6.0 wt% Au	7.9 wt% Au
	Standard Deviation	1.7 wt% Au	0.8 wt% Au
0.75 g/L Au	Average Composition	10.2 wt% Au	9.0 wt% Au
	Standard Deviation	0.3 wt% Au	0.8 wt% Au
1 g/L Au	Average Composition	10.0 wt% Au	11.4 wt% Au
	Standard Deviation	1.7 wt% Au	0.5 wt% Au

Multiple depositions from the same electrolyte are important in terms of the electrolyte's shelf life, especially in industrial applications. Deposits were obtained using a single electroplating electrolyte to determine the changes in deposit composition that result from consumption of the species in electrolyte. A current density of 7.5 mA/cm^2 and a particle loading of 0.75 g/L were utilized (Figure 35) and the amount of Au deposited decreased by approximately 13% after each deposit and began to level off after the 4th deposit at 11.4 wt% Au. The amount of Sn consumed during deposition for the series of experiments was negligible at approximately 2%. In order to counteract the changes in deposit composition with consumption of the submicron Au particles, deposits were attempted with additional submicron Au particles introduced after each deposition. A current density of 7.5 mA/cm^2 and a particle loading of 0.75 g/L were utilized for these depositions (Figure 36). Deposit composition remained approximately constant (ranging from 4.88 to 6.5 wt% Au).

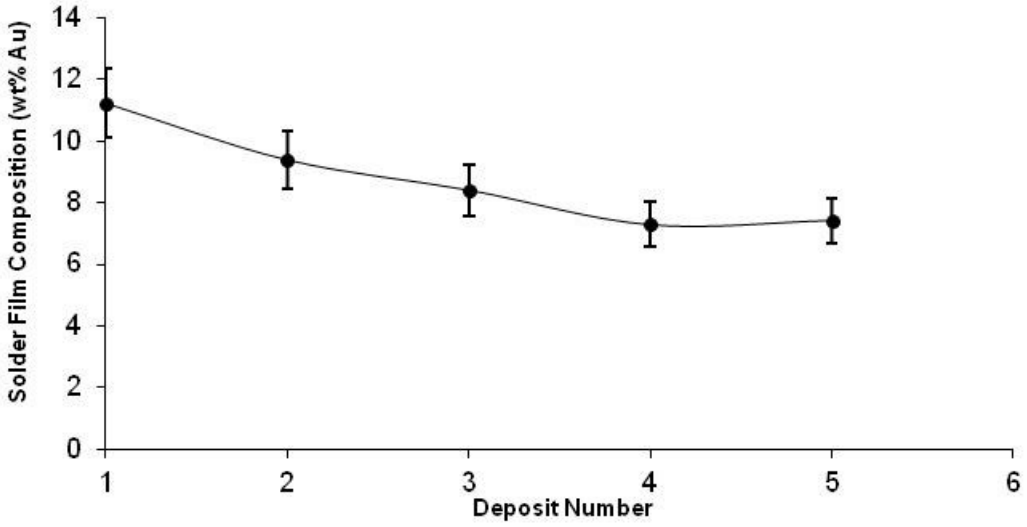

Figure 36: The effect of multiple depositions from the same electrolyte, without additional submicron Au particles, on deposit composition. The initial electrolyte was composed of 75 g/L $(NH_4)_3HC_6H_5O_7$, 50 g/L $SnCl_2 \bullet 2H_20$ and 0.75 g/L of submicron Au particles. The current density was 7.5 mA/cm^2.

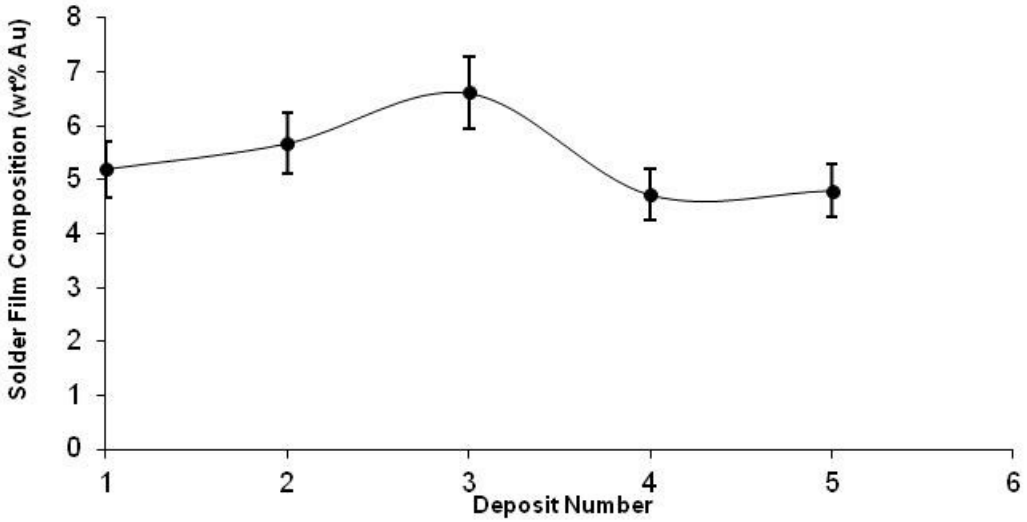

Figure 37: The effect of multiple depositions from the same electrolyte deposits, with additional submicron Au particles introduced after each deposit, on deposit composition. The initial electrolyte was composed of 75 g/L $(NH_4)_3HC_6H_5O_7$, 50 g/L $SnCl_2 \bullet 2H_20$ and 0.75 g/L submicron Au particles. The current density was 7.5 mA/cm^2

Summary. Directly adding submicron Au particles into the Sn plating electrolyte created favorable conditions for producing Sn-rich, Sn-Au solder deposits. Changing the source of the Au in the electrolyte simplified the process, which improved the viability of producing Sn-rich, Sn-Au solder deposits. The addition of submicron Au particles created an electrolyte with repeatable results without compromising the Sn deposit morphology. The deposit chemistry can be further customized by varying the submicron Au particle loading within the electrochemical electrolyte, thus furthering the ability to create multiple depositions from the same electrolyte with repeatable results. The goal of producing simple and cost-effective solder deposits by directly adding submicron Au particles to the Sn electroplating electrolyte shows promise. When producing simple and cost-effective solder deposits, phase formation and the distribution of intermetallics are important considerations. This work is presented in the next chapter.

Chapter 6: Phase Formation in Sn-rich, Sn-Au Deposits

Some electrodeposited samples were stored at room temperature for extended periods (more than 1 week) before their microstructures were characterized using SEM. One such sample is shown in Figure 37. It is evident that interdiffusion has occurred between the Au particles and the surrounding Sn matrix. In the BSE image, grey contrast regions encircle the shrinking Au particles; these have an average atomic number between Au (bright contrast) and Sn (dark contrast). EDS analysis was done on the three contrast regions (Figure 38) and clearly show that the grey contrast regions do indeed contain both Au and Sn, with a Sn:Au atomic ratio close to 4. Comparison with the Au-Sn phase diagram (Figure 39) shows that the phase is Au_4Sn (η phase).

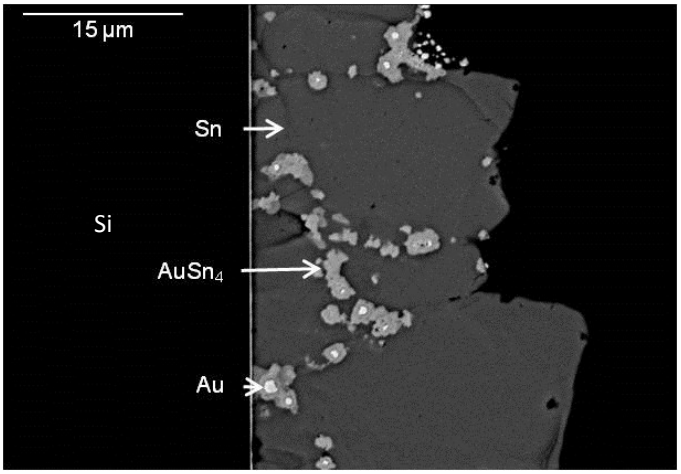

Figure 38: SEM BSE cross section image of Sn-Au deposit after aging for 2 weeks at room temperature. Interdiffusion between Sn and the Au nanoparticles is evident. The electrolyte contained 75 g/L $(NH_4)_3HC_6H_5O_7$ and 50 g/L $SnCl_2•2H_20$, with 0.75 g/L of Au particles, and deposition was done for 90 min at 7.5 mA/cm^2.

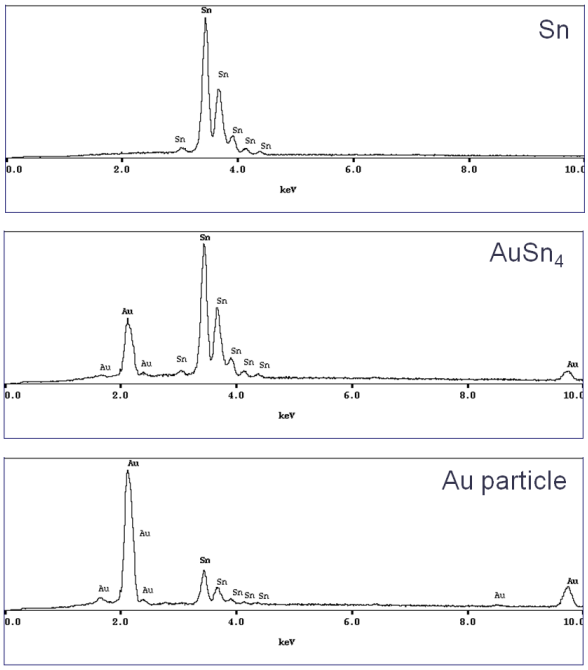

Figure 39: EDS analysis of the different phases present in the sample from Figure 38.

Solid state reaction of Au and Sn was further studied by aging the deposits at elevated temperatures below the eutectic temperature. Samples were aged at 100°C, 150°C ,and 200°C for a period of 1 min in a reducing atmosphere to prevent oxidation of the Sn. BSE images of the aged samples, in plan-view surface and cross-section orientations are shown in Figure 40. Aging the deposits resulted in further consumption of the submicron Au particles to form additional $AuSn_4$. In addition, the Au seed layer reacted with Sn to form $AuSn_4$. The embedded Au particles have been almost completely consumed after the 200°C anneal. Gold particles present on the deposit surface only partially reacted with the Sn matrix upon aging. Incomplete consumption of the surface Au particles may be due to deposit exposure to oxygen after electrodeposition, resulting in oxidation of the Sn surface. The oxide layer could act as a diffusion barrier.

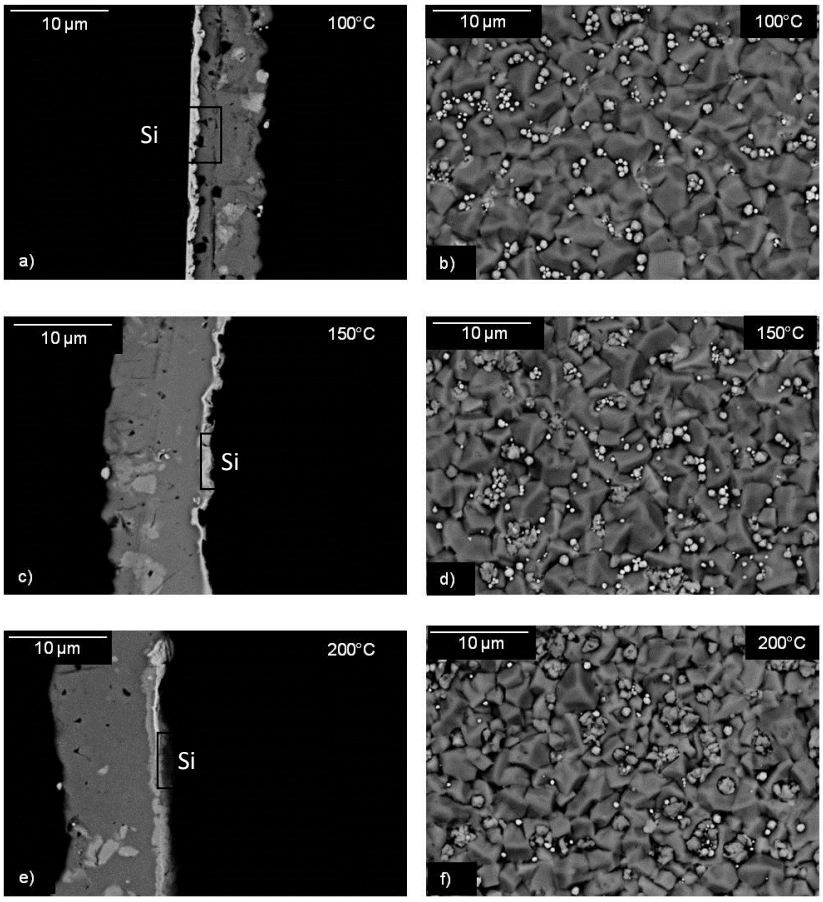

Figure 40: SEM BSE images (cross-section and plan-view) of Sn-Au deposits after aging at elevated temperatures below the eutectic temperature. The deposit in images (a) and (b) was exposed to 100°C for 1 min. The deposit in images (c) and (d) was exposed to 150°C for 1 min. The deposit in images (e) and (f) was exposed to 200°C for 1 min.

Additional samples were investigated at temperatures above the eutectic temperature (~232°C). Reflow was used to ensure complete reaction between the submicron Au particles and Sn matrix, and was done in a reducing atmosphere at temperatures of 250°C, 260°C, and 270°C (Figure 40). Analysis of the reflowed samples revealed similar interactions between the submicron Au particles and the Sn matrix as well as between the Au seed layer and the Sn matrix. Incomplete reaction between the surface Au particles and the Sn matrix is still evident even at elevated reflow temperatures.

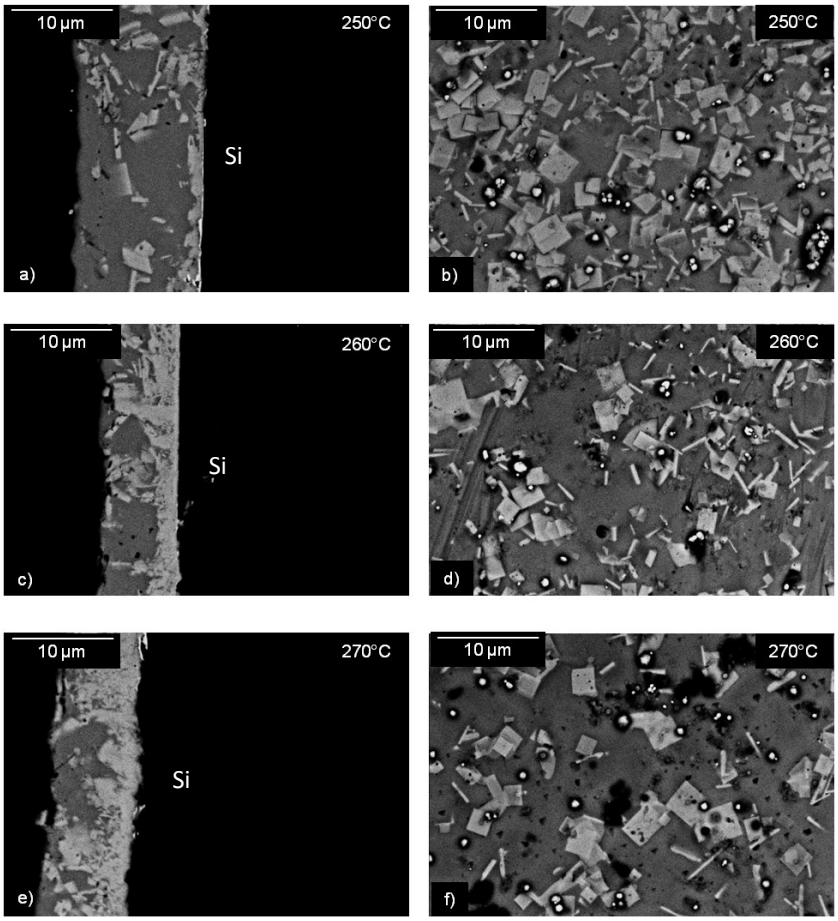

Figure 41: SEM BSE images of samples annealed above the eutectic temperature. The deposit in images (a) and (b) was heated to 250°C for 1 min. The deposit in images (c) and (d) was heated to 260°C for 1 min. The deposit in images (e) and (f) was heated to 270°C for 1 min.

Phase distribution and composition. The distribution and composition of phases after reflow is important to the overall performance of the solder film. Therefore, samples were analyzed to determine the final composition. An electrodeposited sample (with 10 wt% Au) after reflow (250°C for 1 min.) is shown in Figure 40. After reflow, the reflowed layer composition was 24 wt% Au which is hypoeutectic. The excess Au comes from the Au seed layer which is incorporated in the solder during reflow. Two regions are highlighted in the low magnification image in Figure 40 and labeled as (a) and (b). Region (a) is made up of the two

eutectic phases ($AuSn_4$ (brighter contrast) and Sn (darker contrast) – see phase diagram in Figure 41). Region (b) is predominantly $AuSn_4$ (bright contrast) with smaller amounts of Sn.

In order to obtain the eutectic composition (10 wt% Sn) after reflow, samples with the same composition as in the previous paragraph were sonically washed after deposition. The sonically washed samples were then reflowed at 250°C for 1 min (Figure 41). The majority of the surface Au particles were removed from the deposit, thereby reducing the total Au content in the deposit. The remaining Au particles and interaction with the Au seed layer resulted in a final composition of 9.88 wt% Au. An overview of the phase distribution at low magnification is shown in Figure 42a. A high-magnification image of the area indicated by the circle in Figure 42a is shown in Figure 42b. The high magnification image shows a characteristic eutectic structure of $AuSn_4$ and Sn with a few isolated $AuSn_4$ particles. Cross-sectional analysis was also carried out of the sample shown in Figure 43. Figure 43 and 43b show the phase distribution for the reflowed sample at the edge and centre of the solder film, respectively. At the edge of the sample (Figure 43a) the eutectic microstructure is evident. At the center of the film there are isolated $AuSn_4$ particles within the eutectic matrix (Figure 43b).

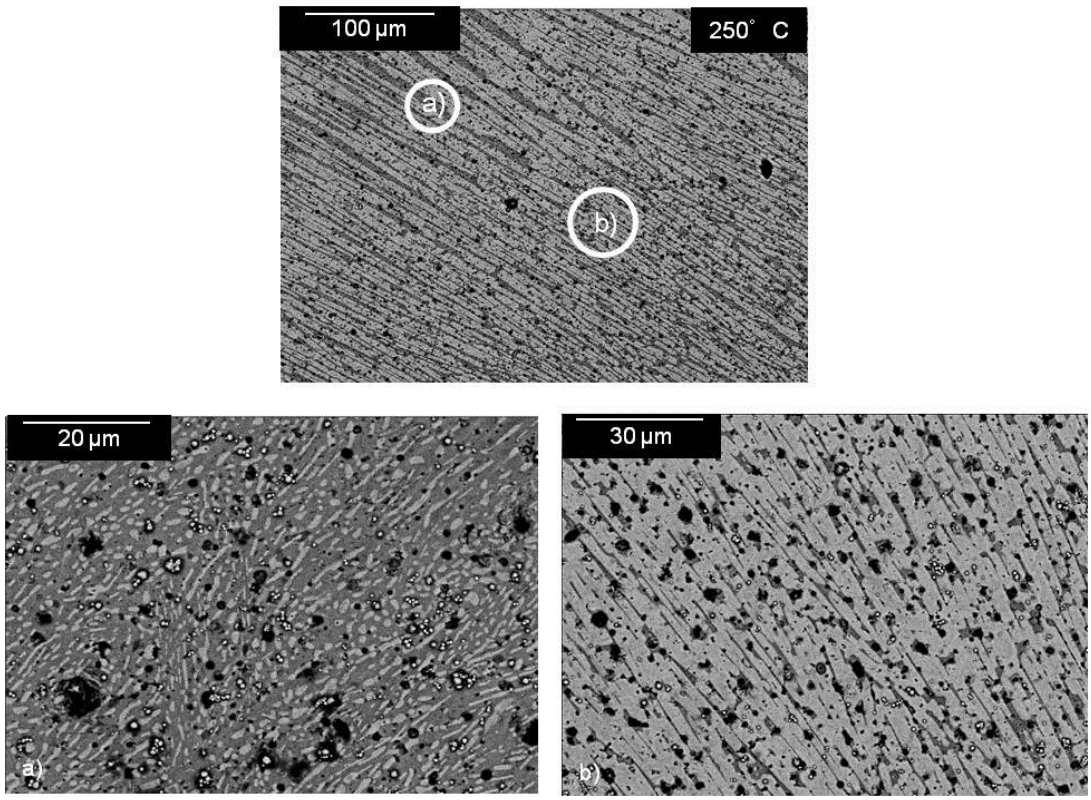

Figure 42: SEM BSE images of a sample deposited using a particle loading of 0.75 g/L Au at a current density of 7.5 mA/cm^2. The sample initially had an as deposited composition of 10 wt% Au and after reflow at 250°C for 1 min the final composition was 24 wt% Au. Images denoted as (a) and (b) are higher magnification images of the two different types of structures visible in the deposit.

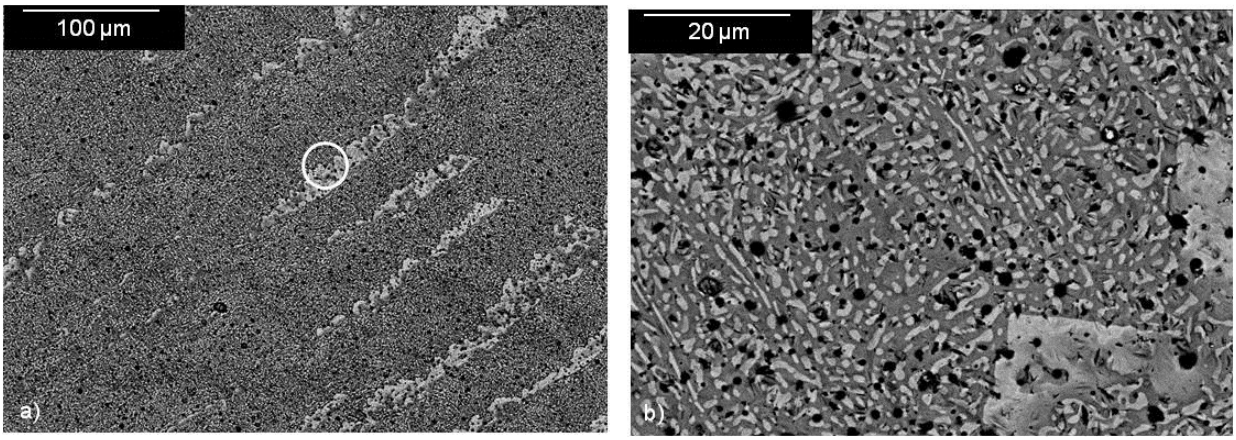

Figure 43: SEM BSE images of a sample the was deposited using a Au particle loading of 0.75 g/L and a current density of 7.5 mA/cm^2. The sample had an as deposited composition of 4.56 wt% Au and after reflow at 250°C for 1 min the final composition was 9.88 wt% Au. The sample was subjected to a sonic wash prior to reflow. Image (a) is a low-magnification image and image (b) is a higher magnification image of the circled region in image (a).

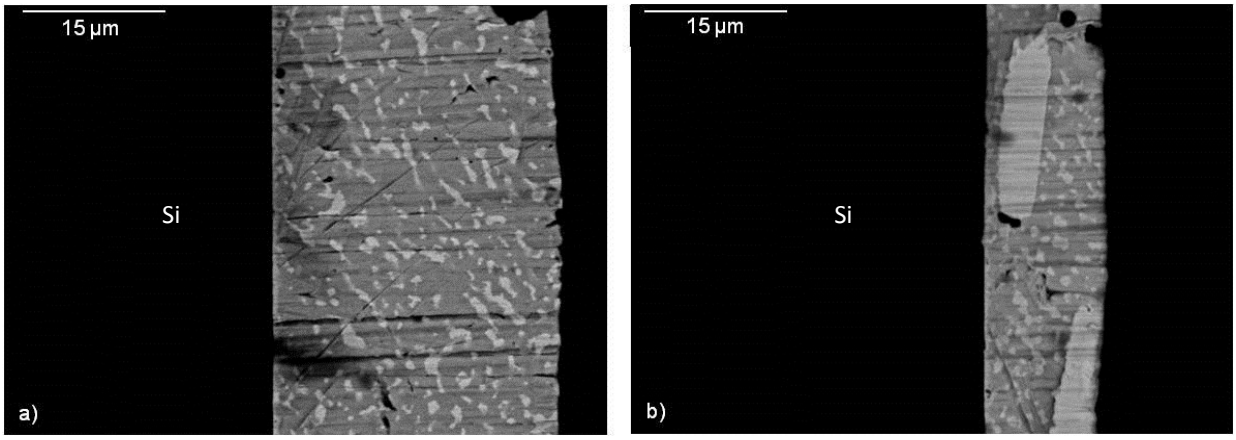

Figure 44: SEM BSE cross-sectional images of a solder film that has undergone a sonic wash process before reflow. Images (a) and (b) are located at the edge and center of the deposit, respectively.

Summary. Phase formation and distribution of the intermetallic $AuSn_4$ will affect the viability and lifetime of Sn-rich, Sn-Au solder films. Interactions between submicron Au particles and the Sn matrix occurred readily at room temperature. The intermetallic $AuSn_4$

formed around the deposited Au particles, which were located along the grain boundaries of the electrodeposited Sn. Gold particles deposited on the surface did not react with the Sn matrix. Aging the deposits at elevated temperatures below the eutectic temperature increased the amount of interaction between the submicron Au particles and the Sn matrix, further driving the reaction and increasing the amount of intermetallic $AuSn_4$ formed in the deposit. Additionally, aging the deposits caused the intermetallic $AuSn_4$ to form at the interface between the Au seed layer and the Sn matrix. Reflow of the Sn-rich, Sn-Au solder deposit was carried out to ensure complete interaction of the submicron Au particles and the Sn matrix. Complete interaction of deposited eutectic Sn-rich, Sn-Au films with the Au seed layer produced a hypoeutectic composition with a high concentration of intermetallic $AuSn_4$. Sonic cleaning of composition deposits reduced the as-deposited composition to 9.88 wt% Au. Reflow of sonically cleaned deposits generated a eutectic composition and microstructure after reflow. The goal of producing simple and cost-effective eutectic solder films using direct addition of submicron Au particles to a simple Sn electrolyte shows promise.

Chapter 7: Conclusions and Future Work

Final Conclusions

The Sn-rich eutectic alloy (90 wt% Sn) in the Au-Sn system offers a potentially cheaper alternative to the Au-rich eutectic alloy (20 wt% Sn) for optoelectronic and microelectromechanical systems (MEMS) device packaging and may be applicable as a Pb-free solder for microelectronic packaging. A life cycle analysis of Au-Sn electrodeposition development in industry and the scientific background of electrodeposition was provided. Specific details were given regarding the history of solders, trends in the field, and initiatives to further develop solders. Considerations regarding design, toxicity and public health impact, availability of raw materials, and environmental impacts when making decisions in selecting alternative materials were discussed.

A simple electrodeposition method was utilized to fabricate Sn-rich, Au–Sn solder films, including the eutectic composition. The electrolyte consisted of a electrolyte of Sn chloride and ammonium citrate. Gold was added to the electrolyte in the form of either a Au nanoparticle (<20 nm) suspension, prepared with Na citrate, or by directly adding Au powder (500–800 nm particles). Historically, electrodeposition has proven to be an economical and valid technology for producing deposits that may be categorized depending on their main function; i.e., to improve the appearance of a part, impart a protective surface on a part, or modify the chemical or physical properties of a part's surface.

Initially, the co-deposition of Au nano-particles mixed with a Sn plating electrolyte was explored to produce a viable Sn-rich, Sn-Au solder deposit. Direct addition of tri-ammonium citrate and Sn chloride to the Au nano-particle suspension produced a relatively smooth Sn layer. Changes to the electrochemistry of the electrolyte (i.e., the concentration of the nano-Au suspension and the Sn solution) caused an increase in the amount of the Au nano-particles deposited at the expense of the film's morphology. Additives improved the deposit morphology but inevitably prevented incorporation of the Au nano-particles into the deposit. Since the relationship between the Sn morphology and incorporation of the Au nano-particles was complex, a decision was made to develop a different electroplating bath.

In the second approach, the direct addition of Au submicron particles into an Sn plating electrolyte created favourable conditions for producing Sn-rich, Sn-Au solder deposits. Changing the source of the Au in the electrolyte simplified the electrochemistry, which improved the viability of producing Sn-rich, Sn-Au solder deposits. The addition of submicron Au particles created an electrolyte with repeatable results without compromising the Sn morphology.

Phase formation and distribution of the intermetallic $AuSn_4$ will affect the viability and lifetime of Sn-rich, Sn-Au solder films. Interactions between submicron Au particles and the Sn matrix occurred readily at room temperature. Initial intermetallic $AuSn_4$ formed around the deposited submicron Au particles along the grain boundaries of deposited Sn, while submicron Au particles deposited on the surface did not react with the Sn matrix. Aging the deposits at elevated temperatures below the eutectic temperature increased the amount of interaction between the submicron Au particles and the Sn matrix, further driving the reaction and increasing the amount of intermetallic $AuSn_4$ formed in the deposit.

Reflow of the Sn-rich, Sn-Au solder deposit was carried out between 250°C and 270°C. During the reflow process complete interaction of deposited eutectic Sn-rich, Sn-Au films with the Au seed layer occurred. Reflow of the as deposited samples produced a hypoeutectic composition with an excess of intermetallic $AuSn_4$. Samples that were sonically cleaned before reflow had the composition of 9.88 wt% Au.

The Sn-rich, Sn-Au solder composition is not currently used in industry. Thus, there is an opportunity to explore an alternative composition for solder joints for optoelectronic and MEMS applications.

Future Work

A more defined statistical analysis and probabilistic assessment could be completed to further define the viability of Au submicron particle additions into a Sn electrolyte. By determining the most effective factors influencing the deposit composition and plating rate a statistical analysis could be complete alongside the deterministic assessment. The resulting assessment could be used to develop a predictable and consistent method to deposit Sn-rich, Au-Sn deposits.

The next focal point in studying Sn-rich, Sn-Au solder films could be determining the capability of creating a bond and the resulting strength of the bond. Phase formation and distribution of the bonded substrates could be studied by performing pull or shear tests to determine the bond strength of the reflowed Sn-rich, Au-Sn deposits.

References

American Society for Metals, Binary Alloy Phase Diagrams, Alloy Phase Diagrams Vol 3, ASM Handbook, ASM International, 2012.

Allebby, B., Artaki, I., Carroll, T., Dahringer, D.W., Degani, Y., Fisher, J.R., Freund, R.S., Gherman, C., Graedel, T.E., Lyons, A.M., Melton, C., Munie, G.C., Schoenthaler, D., Plewes, J.T., Socolowshi, N., Solomon, H. An Assessment of the Use of Lead in Electronic Assembly. National Surface Mount Council, IPC, 1992.

Bard, A.J., Faulkner, L.R., Electrochemical Methods: Fundamentals and Applications. John Wiley & Sons, Inc., 2001.

Barkey, D.P; Wu, Q; Keigler, A.; Liu, Z.; Electrocodeposition of Silver Particles with Tin for Fabrication of Lead-Free Solder Bumps. ECS Transactions, 1, 13, 43-51, 2006.

Boustedt, K., GHz Flip-Chip: An Overview, Electronic Component and Technology Conference, 297-302, 1998.

Chaung, R.W., Lee, C.C., A Fluxless Au-Sn Bonding Process of Tin-Rich Compositions Achieved in Ambient Air, 52nd Electronic Components and Technology Conference, 134-137, 2002.

Doesburg, J., Ivey, D.G., Microstructure and Preferred Orientation of Au-Sn Alloy Plated Deposts, Materials Science and Engineering B, in press, 21 manuscript pages, 2000.

Djurfors, B., Ivey, D.G., Microstructural Characterization of Pulsed Electrodeposited An/Sn Alloy Thin Films, Materials Science & Engineering B, B90, 3, 309-320, 2002.

Foulke, D.G., Metal Finishing, 67, 4, 50, 1969.

Foulke, D.G., in: Reid, F.H., Goldie, W., Gold PlatingTechnology Chapter 7, Electrochemical Publications, 52, 1974.

Gamalski, J., A European Perspective from a Global OEM, IPC/Jedec Conference on Lead Free Electronic Components and Assemeblies, 2002.

Goldstein J.L., Scanning Electron Microsopy and X-ray Microanalysis, Springer Science & Business Media, LLC, 2003.

He, A., Ivey D.G., Electrodeposition of Tin: A Simple Approach, Journal of Materials Science: Materials in Electronics, 19, 6, 553-562, 2008.

He, A., Ivey, D.G., Electrodeposition of Sn and Au-Sn alloys from a Single Non-Cyanide Electrolyte. Journal of Electronic Materials, 23, 12, 2186-2193, 2012.

Jeong, G.H., Kim, J.H., Lee, D., Suh, S.J., Microstructure and Composition of Au-Sn Eutectic Solder Electroplated from a Single Solution, Materials Research Society Symposium Proceedings, 894, LL03-16.l-LL03-16.5, 2006.

Kallmayer, C., Lin, D., Kloeser, J., Oppermann, H., Zakel, E., Reichl, H., Fluxless Flip-Chip Attachment Techniques using Au/Sn Metallurgy. IEEE:CPMT International Electronics Manufacturing Technology Symposium, 20, 1995.

Kallmayer, C., Lin, D., Oppermann, H., Kloeser, J., Weib, S., Zakel, E., Reichl, H., Fluxless Flip-Chip Soldering using Eutectic Gold-Tin System: A Comparison between self-alignment and thermode-bonding, Proceedings of the 10th European Microelectronics Conference, 440, 1995.

Kim, J., Lee, C.C., Fluxless Sn-Rich Sn-Au Flip-Chip Bonding Using Electroplating Process. 10th International Symposium on Advanced Packaging Materials: Processes, Properties and Interfaces, 164 (2005).

Kim, J., Kim, D., Lee, C.C., Fluxless Flip-Chip Solder Joint Fabrication Using Electroplated Sn-Rich Sn-Au Structures. IEEE Transactions on Advanced Packaging, 29, 473, 2006.

Kim, J., Lee C.C., Fluxless Wafer Bonding with Sn-rich Sn-Au Dual-Layer Structure, Materials Science and Engineering, A, 417, 143-148. 2006.

Kim, J.S., Wang, P.J., Lee, C.C., Fluxless Hermetic Lid Sealing Using Electroplated Sn-Rich Solder, IEEE Transactions on Components and Packaging Technologies, 31, 3, 2008.

Kubota, N., Horikoshi, T., Sato, E., Electrodeposition of Gold-Tin Alloys from Pyrophosphate Solution, Journal of Metal Finishing Society of Japan, 34, 37-43, 1983.

Ku, A., Lead-Free Solders: Issues of Toxicity, Availability and Impacts of Extraction, 53rd Electronic Components and Technology Conference Proceedings, 47-53, 2003.

Le Fevre, P.J.F., Environmental Issues in Power Electronics, IEEE Applied Power Electronics Conference and Exposition, 1, 121-125, 2002.

Lee, C.C., Chuang, R.W., Fluxless Non-Eutectic Joints Fabricated Using Gold-Tin Multilayer Composite, IEEE Transactions Components and Packaging Technologies, .26, n2, 416-422, 2003.

Lowenhein, F.A., Modern Electroplating, 3rd Edition. Wiley-Interscience. 1974.

McFarland, A.D., Haynes, C.L., Mirkin, C.A., Van Duyne, R.P., Godwin, H.A., Color My Nanoworld. Journal of Chemical Education, 81, 4, 544A, 2004.

Morawej, N., Ivey, D.G., A statistical design of experiments (DOE) approach to improving the process for electrodeposition of gold-tin alloys from chloride-based solution, Journal of Applied Surface Finishing, 2, 3, 220-225, 2007.

Nimmo, K., Review of European Legislation and Lead Free Technology Roadmap, IPC/Jedec Conference on Lead Free Electronic Components and Assemblies, 2002.

Paunovic, M., Schlesinger, M., Fundamentals of Electrochemical Deposition 2nd Edition. John Wiley & Sons, Inc., 1998.

Paunovic, M., Schlesinger, M., Modern Electroplating, 4th Edition. The Electrochemical Society, Inc., 2000.

Raub, C.J., Knodler, A.,Lendvay, L., Plating, 63, 35, 1976.

Reid, F.H., Goldie, W., Gold Plating Technology. Electrochemical Publications, 1974.

Sun, W., Ivey, D.G., Development of an electroplating solution for Codepositing Au–Sn Alloys, Materials Science and Engineering, B65, 111, 1999.

Sun, W., Ivey, D.G., Microstuctural Study of Co-Electroplated Au/Sn Alloys, Journal of Materials Science, 36, 3, 757-766, 2001.

Tanabe, Y., Hasegawa, N., Odaka, M., On the microstructure and the phase of Electroplated Au-Sn and Ag-Sn alloys, Journal of Metal Finishing Society of Japan, 34, 452-458, 1983.

Tang, W., He, A., Liu, Q., Ivey, D.G., Fabrication and Microstructures of Sequentially Electroplated Au-rich, Eutectic Au/Sn Alloy Solder, Journal of Electronic Materials, 37, 837, 2008.

Tang, W., He, A.,, Liu, Q., Ivey, D.G., Room Temperature Interfacial Reactions in Electrodeposited Au/Sn Couples, Acta Materalia, 56, 5818-5827, 2008.

Trumble, B., Get the Lead Out, IEEE Spectrum, 55-60, 1998.

Turbini, L., Munie, G., Bernier, D, Gamaiski, J. Bergman, D., Examining the Environmental Impact of Lead-Free Soldering Alternatives, Australian Electronics Engineering, 34, 2, 12-18, 2001.

Volk, F., U.S. Patient, 2,812,229, 1957.

Wenzel, H., Hauschild, M., Alting, L., Environmental Assessment of Products, London, UK: Chapman & Hall, 1997.

Zakel, E., Reichl, H., in: J. Lau Edition, Flip-Chip Technologies Chapter 15, McGraw-Hill, 415, 1995,

Zhang, Y., Tin and Tin Alloys for Lead-Free Solder, Modern Electroplating, 5th Edition, John Wiley & Sons, Inc., 139-164. 2010.

Zhou, X., Schoenung, J.M., An Integrated Impact Assessment and Weighting Methodology: Evaulation of the Environmental Consequences of Lead-Free Solder Alternatives, 16th IEEE International Symposium on Electronics and the Environment

Zoski C.G., Handbook of Electrochemistry, Elsevier B.V.,2007